Deanship of Graduate Studies

Al-Quds University

Comparison between Monte Carlo Simulations, The estimates of the Mean Particle Theory and Observations of H^+ and O^+ Outflows at High Latitudes.

May Rajab Halaika

M.Sc. Thesis

Jerusalem-Palestine

1444 / 2023

Comparison between Monte Carlo Simulations, The estimates of the Mean Particle Theory and Observations of H^{+} and O^{+} Outflows at High Latitudes.

Prepared by:

May Rajab Halaika

B.Sc.: Physics. Palestine Polytechnique University. Palestine.

Supervisor: Prof. Dr. Imad A. Barghouthi

A thesis submitted in partial fulfillment of requirements for the degree of master of physics, Al-Quds University

1444/2023

Al-Quds University

Deanship of Graduate Studies

Physics Department

Thesis approval

Comparison between Monte Carlo Simulations, The estimates of the Mean Particle Theory and Observations of H^+ and O^+ Outflows at High Latitudes.

Prepared by: May Rajab Halaika

Registration No.: 21920065

Supervisor: Prof. Dr. Imad A. Barghouthi

Master thesis submitted and accepted, Date: 22 / 05 / 2023

The names and signatures of the examining committee members as follows:

1- Head of Committee: Prof. Dr. Imad A. Barghouthi Signature

2- Internal Examiner: Dr. Husain Alsamamra Signature

3- External Examiner: Dr. Mustafa AbuSafa Signature

Jerusalem-Palestine

1444 / 2023

Dedication

To my parents

To my sisters and brother

To my friends

Declaration:

I certify that this thesis submitted for the degree of master is the result of my own research, except where otherwise acknowledged, and that this thesis, neither in whole or in part, has been previously submitted for any degree to any other university or institution.

The work was done under the supervision of Prof. Dr. Imad A. Barghouthi from physics department-Al-Quds University.

Name: May Rajab Halaika

Signed: May halaika

Date: 22 / 05 / 2023

Acknowledgement

I would like to express my sincere thanks to my instructor and supervisor Prof. Dr. Imad A. Barghouthi for his guidance, assistance, advice and constant encouragement during research.

My deepest gratitude to my teachers; the staff of physics Department at Al-Quds University for their continuous support during my master’s study.

Abstract

In this thesis we make a comparison between the results of Monte Carlo simulations, mean particle theory, and observations in different regions of earth magnetosphere (aurora, polar wind, central polar cap and, cusp) for H^+ and O^+ ions outflow at high latitudes and altitudes. We present altitude profiles for mean perpendicular energy $W_{\perp}$, mean parallel energy $W_{\|}$ and, total mean energy W_{total}. Monte Carlo simulations are obtained by using Barghouthi model [Barghouthi, 2008], mean particle theory estimates are obtained by using Retterer et al. [1987a], and observations are obtained from different available studies. As a results of comparisons in different regions we have found that; 1) Monte Carlo simulations and Mean particle theory gives similar results in auroral regions and produce no agreement in polar wind region, 2) comparison with observations in polar wind region and auroral region gives excellent agreement in aurora and good agreement in polar wind, 3) it is appropriate to use altitude and velocity diffusion coefficients in auroral and polar wind regions, because of that we have obtained reasonable results, 4) in the central polar cap and cusp we have obtained excellent agreement for both methods and observations, 5) due to these comparisons we can claim that the wave length of the electromagnetic wave existed in those regions is 8km.

Table of contents:

List of Figures

CHAPTER ONE

INTRODUCTION

1.1 Introduction

Many studies are developed to investigate the ions outflow from Polar Regions of the earth to outer space, which necessitated the building of many models and hypotheses to know the behavior of these ions and the factors that affect them, in addition to all their characteristics such as temperature, velocity and others. One of the most prominent and important of these models was Barghouthi model, who was able to provide results that are very close to the data that were monitored in space at different altitudes. Research and development processes are still going on to gather as much information as possible about the flow of these ions, including the energy and their components, which will be the core topic for us in this research, which helps in understanding the nature and components of space. Therefore, many researches have been presented in this regard on various topics.

Chang et al. [1986] built the most basic model to explain the ion flux, which describes the perpendicular heating of ions in a dipole magnetic field. They also proposed that the intense broad band electric field fluctuations observed in the frequency range of (0-100 Hz) could be the cause of the transverse activation of ions through cyclonic resonance heating with left-handed polarized electromagnetic waves. Additionally, using a set of equations that described the motion of the ion in the geomagnetic field, they determined the parallel and perpendicular energies in accordance with the mean particle theory.

Retterer et al. [1987a] demonstrated how oxygen ions form conics in the auroral zone of the earth and used the diffusion equation to explain ion distributions that could be solved by using the Monte Carlo method. The comparison between Monte Carlo and mean particle theory at various heating rates $2mD_{\perp}$ made this study the first to compare an observed conic with any theoretical model.

Using Monte Carlo simulation, Barakat and Barghouthi [1994a] investigated the impact of wave particle interaction (WPI) on the polar wind flow. The electrostatic field, gravity, and geomagnetic field lines are all considered in the model. Only the results relating to O^{+} were given, even though the plasma also contained H+ and electrons. The normalized quasilinear velocity diffusion rate $\widetilde{D_{\perp}}(O^{+})$ was modified across a broad range in response to observations, and the distribution function $f(O^{+})$and its velocity moments were calculated.

Barakat and Barghouthi [1994b] developed the study effect of wave particle interactions (WPI) on the plasma outflow in the polar wind by Monte Carlo simulation. They explained the behavior of the ion (only H^{+}) distribution function as well as the profiles of its moments (density, drift velocity, temperatures. etc.) and they found as WPI strength increases the ion drift velocity increases and its density decreases, the parallel temperatures firstly decreases and then will increase $T_{\parallel}(H^{+})$, the perpendicular temperatures $T_{\perp}(H^{+})$ increasing .

By using Monte Carlo simulation, Barakat and Barghouthi [1994b] produced a study of the impact of wave particle interactions (WPI) on the plasma outflow in the polar wind. As WPI strength increases, they discovered that the ion drift velocity increases and its density decreases, the parallel temperatures first decrease and then increase $T_{\parallel}(H^{+})$, and the perpendicular temperatures $T_{\perp}(H^{+})$ increase. They also explained the behavior of the ion (only H^{+}) distribution function as well as the profiles of its moments (density, drift velocity, temperatures, etc.).

Barghouthi [1997] presented the impact of altitude-dependent WPI on $H^{+}$and O^{+} ion outflow in the polar cap and auroral zone using the Monte Carlo simulation. Additionally, he investigated the model by comparing the estimations from the mean particle theory with the data from the auroral region produced by Monte Carlo simulation. Despite the absence of supporting observations, there was strong agreement between the two methods.

[Bouhram et al., 2002, 2003a , 2003b , 2004] examined the cusp cleft region's transverse heating and ion outflow.

Barghouthi et al. [2006] concentrated on the Monte Carlo simulation of toroidal $H^{+}$and O^{+} velocity distributions at high altitudes equatorward of the cusp By using a suitable form for $D_{\perp}$. The findings of the Monte Carlo simulations of the toroidal $H^{+}$and O^{+} velocity distributions and $H^{+}$and O^{+} ion temperatures were compared to the toroidal $H^{+}$and O^{+} ion distributions and $H^{+}$and O^{+} ion temperatures that were really observed at high altitudes equatorward of the cusp [Huddleston et al., 2000].

Barghouthi [2008] employed the Monte Carlo simulation to determine the temperatures and velocity distributions of $H^+$and O^+ ions at high altitudes in the equatorward portion of the cusp using various forms of the velocity diffusion coefficient, $D_\perp(r, v_\perp)$ (RCC model, Bouhram model, and Barghouthi model). These models' outputs have been contrasted with the matching Huddleston et al. [2000] observations.

Waara et al.[2010] were shown a case study of considerable heating of outflowing oxygen ions at high altitude (12 R_E) above the polar cap (up to 8 keV) perpendicular to the geomagnetic field. The distribution functions' shape suggests that the majority of the heating takes place locally within (0.2–0.4 R_E) of altitude). They discovered that It is unlikely that the locally observed wave fields can explain the observed ion energization because there are several events at lower altitudes. Furthermore, it is unlikely that the ions have migrated from an energizing location nearby to the observation site. This shows that at high altitudes, additional, fundamentally distinct ion energization pathways exist. One explanation is that the ions' magnetic moment is not conserved, which would lead to slower outflow velocities and a longer ion energization period.

Waara et al. [2011] they provide the average values of coefficient which can be used to describing the diffusion in ion velocity at various altitude which can be consider a useful way to study ion outflow behavior and their energies. The average energies of O^+ can be explained by the observed average wave in high altitudes (8 - 15 R_E) in cusp and mantle regions according their test particle calculations. They expected the relation between electric and magnetic field spectral density according to their results and the diffusion confection of O^+ increases with altitude.

Barghouthi et al. [2012] they compared the simulation of ion outflow in two different region which are polar wind and auroral region based on the Barghouthi model. Also they computed the perpendicular and parallel temperature of ion, ion density, and ion drift velocity and ion velocity distributions at various altitudes where in the auroral region. 1.2 R_E to 10 R_E and the polar wind 1.7R_E to 10 R_E . They also discovered that wave particle interactions have a greater impact on the auroral zone than they do on the polar wind region, and that they have a greater impact on the energizing of O^+ ions than H^+ ions.

Barghouthi et al. [2016] updated the Monte Carlo model by taking into account the effect gravity, am bipolar electric field, centrifugal acceleration, mirror force and wave particle interaction to study the O^+ and H^+ ions outflow above the polar cap. And they changed various parameters like (centrifugal acceleration, diffusion coefficients, and boundary conditions at lower-altitude) and compared their results with the observations obtained by the devices on board Cluster spacecraft which are agree with observed data with accurate values of diffusion coefficients and lower-altitude boundary conditions.

1.2 Objectives of the study

The main objectives of the present study are to:

1) Using the Monte Carlo simulation to study the behavior of both ($H^+$and O^+) ions outflow and how the ion density, drift velocity, parallel and perpendicular temperatures varies with high altitude and using these data to find the mean perpendicular $W_\perp$ energies, mean parallel $W_\parallel$ energies and the total energies W_{total}.
2) Using different diffusion coefficients values according to the region in space to estimate the mean parallel energies $W_\parallel$, mean perpendicular energies $W_\perp$ and total energies W_{total}.
3) Making a comparison between Monte Carlo simulations, mean particle theory estimates, and observations at different regions in earth magnetosphere.

CHAPTER TWO

THEORETICAL FORMULATIONS

2.1 Introduction

In this chapter, we will introduce 1) the regions of studies, auroral region, polar wind region, polar cap, central polar cap, and cusp, 2) Monte Carlo technique and Barghouthi model, and 3) the mean particle theory.

2.1.1 Auroral Region:

Typically, high-latitude atmospheric emissions known as auroras are the result of intense charged particles precipitating from a planet's magnetosphere. Ground-based observatories, Earth-orbiting satellites like the International Ultraviolet Explorer (IUE) and Röentgensatellit (ROSAT), as well as orbiting spacecraft platforms like Galileo, have all recorded auroral emissions from the giant planets at wavelengths in the X-ray, ultraviolet (UV), visible, infrared (IR), and radio ranges. Radio and X-ray auroras are beam emissions, created by the precipitating species themselves, while UV, visible, and IR auroras are atmosphere emissions, formed or initiated when ambient atmospheric species are stimulated by collisions with the precipitating particles. The emissions at various wavelengths offer distinct and complementary information on the important physical processes taking place in the atmosphere and magnetospheric areas where they originate, which is accessible to remote sensing [Bhardwaj and Gladstone, 2000].

The interaction of intense electrons and protons that are precipitating with the upper atmosphere produces aurora. It typically appears around the geomagnetic poles as continuous, hazy ovals of light when viewed from space. There are also smaller, isolated auroral areas that are unrelated to the ovals and have unique morphological, spatial, and temporal characteristics [Frey, 2007]. Some of these nearby aurorae are separated from the oval to its pole or equator. Others are situated inside the oval and shine brighter than the diffuse aurora around them. Many of them only happen under favorable solar wind circumstances and interplanetary magnetic field orientations.

The solar wind, a continually expelled stream of electrons and protons from the sun, is one potential source of auroral power. An energy flux of $0.5\,\mathrm{erg}/\mathrm{cm}^2/sec$ is produced in the solar wind by the proton velocity, which is on average 5×10^7 cm/sec and the proton number density close to the planet, which is $5\ \mathrm{particles}/\mathrm{cm}^3$. According to Van Allen [1966], the overall geomagnetic field offers the solar wind a circular frontal region with a radius of around 12 earth radii, resulting in a solar wind power intake of $\sim 3 \times 10^{12}$watt, or about 300 times more than what is needed to sustain an IBC-3 aurora.

From power considerations alone, the solar wind could be the source for any aurora but its role if any, is not yet established. The average energy' of the solar-wind proton is 1.3 keV; and from arguments based on electrical neutrality for the wind, it is expected that the electron and proton velocities are equal, in which case the average electron energy is 0.7 eV, much less than the keV energies of auroral electrons [Van Allen,1966]. (To penetrate through the atmosphere above the aurora and to produce an aurora at the altitudes where they regularly appear, ~ 100 km, primary electrons must have an energy of at least a few keV).

2.1.2 Polar Wind Region

Ion outflows from the polar ionosphere and direct or indirect entry of solar wind plasma are now generally recognized as the magnetosphere's two primary plasma sources. The ionosphere was discovered to be a significant source of magnetospheric plasma after Shelley et al. [1972] finding of O^+ ions in the magnetosphere. One of the primary contributors of the polar ionosphere, a significant and occasionally dominant source of plasma for the magnetosphere, is polar wind.

Due to the early space exploration discoveries of the magnetotail, plasmapause, and atmospheric helium attrition, the pole wind was hypothesized to exist in the late 1960s. The polar wind was initially defined as an ambipolar outflow of hot plasma along "open" geomagnetic field lines from the high-latitude ionosphere to the magnetosphere, primarily made up of electrons and light (H^+ and He^+) ions. Axford [1968] coined the term "polar wind" to denote the supersonic features of the thermal plasma expansion and outflow using the solar wind plasma's supersonic expansion from the solar corona into interplanetary space as an analogy.

The polar wind is the ionosphere of the earth's polar regions' outflow of light ions. The current inquiry focuses on the outcomes of a thorough simulation of the steady state outflow of H^+ and He^+ ions into the magnetosphere's tail regions from the polar ionosphere. H^+ outflow, He^+ outflow, and the collisionless polar wind are considered when analyzing theoretical models of the polar wind [Raitt and Schunk, 1983]. The polar wind is an ambipolar outflow of heated plasma traveling along geomagnetic field lines from the terrestrial ionosphere at high latitudes to the magnetosphere. H^+ , He^+ and O^+ ions predominate in the polar wind plasma, along with electrons. Although it was once thought that O^+ ions only played a significant role at low altitudes, it is now evident from measurements that the polar magnetosphere contains rather high volumes of suprathermal and energetic O^+ ions. Recently, thermal O^+ outflow with H^+ and He^+ ions have been seen at altitudes of 5000–10,000 km [Ganguli, 1996].

2.1.3 Central Polar Cap Region

The region encircling the geomagnetic poise and enclosed by the aurora ovals is known as the central polar cap. On both hemispheres, the polar caps are high-altitude regions with an open magnetic field line that connects to the interplanetary magnetic field. Polar caps from one of the magnetospheric plasma's ionospheric sources are also included [Banks and Holzer, 1968]. This is because of the alleged polar wind, which was initially proposed by theoretical reasoning [Axford, 1968].

2.1.4 Cusp Region

The magnetosheath plasma has direct access to the ionosphere at the polar cusp. Whether the interplanetary magnetic field is pointing north or south, it still persists. The magnetosphere's shape determines where the cusp is located in a non-reconnecting magnetosphere; however, the cusp's placement changes when the magnetosphere re-connects with either a southbound or a northward interplanetary magnetic field. The polar cusp has primarily been explored at low altitudes since it was first identified in 1971 at both low and high altitudes [Russell,2000].

The cusps are crucial areas for the transport of mass and momentum from the magnetosheath to the Earth's magnetosphere. This region also helps the solar wind particles reach directly to the ionosphere .In an open magnetosphere model, magnetic reconnection produces freshly opened field lines that are stocked with magnetosheath ions and convected over this region under a southbound [Dungey, 1961] or northward [Dungey, 1963] IMF. High-altitude cusp regions are closer to reconnection sites than lower-altitude cusp regions because they are close to the magnetosheath.

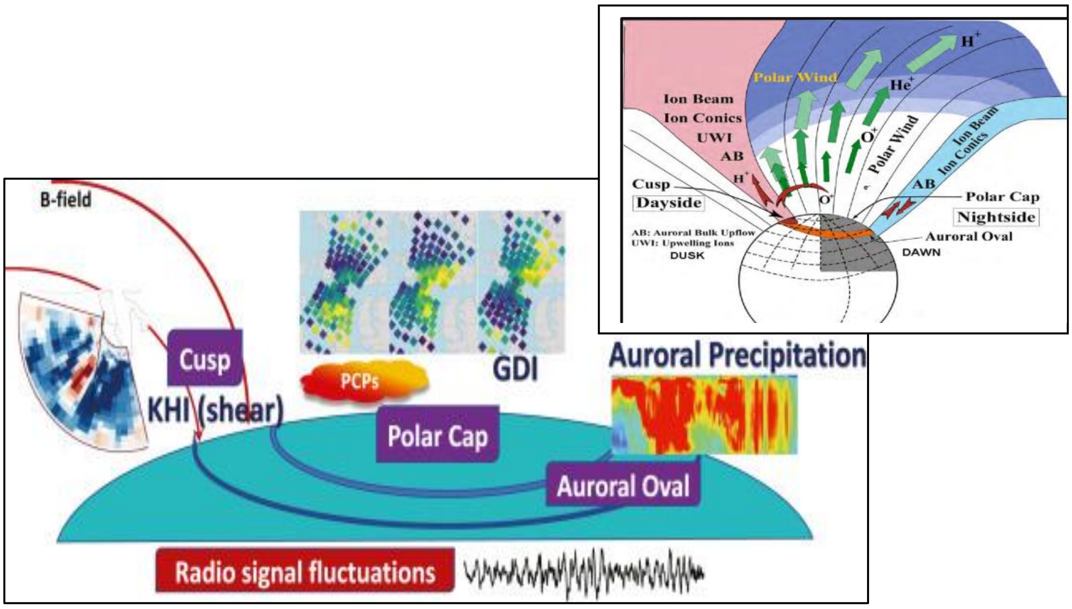

Figure 2. 1. Represent the different regions that we are applying our study over it.
http://ssdoo.gsfc.nasa.gove /education/lectures /fig12.gif

2.2 Monte Carlo Simulation

To simulate random processes, Monte Carlo techniques are employed. The number sequences used in these simulations are 'pseudo-random'. The computationally demanding nature of MC techniques made them more crucial as computer resources grew more affordable and accessible. Since the early 1950s, MC approaches have been used in space physics to simulate the consequences of collisional processes according to Barakat and Schunk [1982], and wave-particle interactions [Barkat and Barghouthi, 1994a,b]. It was shown that the Monte Carlo method is a very efficient method for solving the Boltzmann equation using particle simulation. Due to its uncomplicated technique, basic idea, and capacity to include new features (such as gravity, electric field, geomagnetic field, and various collision models), it is an effective instrument for space plasma physics and a powerful evaluation of results achieved with other mathematical methods. [Barghouthi et al., 2003].

The typical method of the Monte Carlo simulation is to track the motion of a single ion as it is subject to external forces and many collisions, and to continuously check its velocity. Then, different ion time averages of different types are calculated, which may be equal to the appropriate ensemble averages of the system [Barakat et al., 1983].

The following is a practical simulation of ion motion. A randomly generated beginning velocity of an ion is injected into the simulation zone, making sure that it is consistent with the ion velocity distribution function directly beneath the simulation region. An appropriate random number generator is used to determine the amount of time between each pair of subsequent collisions. The classical principles of motion of a charged particle under the influence of gravitational, electric, and geomagnetic fields 25 govern the ion paths during these periods. Another set of random numbers with statistical qualities chosen in accordance with the selected collision model is used to calculate changes in ion velocity caused by collisions [Barakat and Lemaire, 1990]. The behavior of the ion is then recorded using an appropriate grid in velocity space at various elevations in the simulation region. It is assumed that the velocity distribution function of an ion at its center is proportional to the duration an ion spends in each bin, divided by the volume of the bin. Additionally, multiple velocity moments (such as density, drift velocity, temperature, and heat flow...) can be directly determined from the trajectory's component segments.

Ions, electrons, and neutral atoms make up the plasma medium, which includes the polar wind, ionosphere, magnetosphere, and plasmasphere. It is exceedingly challenging to comprehend how these species move while being affected by the geomagnetic field, gravitational field, polarization electric field, and interactions between them. However, Winkler et al. [1992]

The motion of the plasma's constituents and some interactions between plasma species can be precisely defined via Monte Carlo simulation. When working with plasma, it is practical to characterize each species using a different velocity distribution function. f_s ($\mathbf{v}_s$, $\mathbf{r}_s$,t) .

The velocity distribution function is defined such that f_s ($\mathbf{v}_s$, $\mathbf{r}_s$,t)$d\mathbf{v}_s d\mathbf{r}_s$ represents the number of particles of species s which at time t have velocity between $\mathbf{v}_s$and $\mathbf{v}_s+ d\mathbf{v}_s$ and positions between $\mathbf{r}_s$and $\mathbf{r}_s + d\mathbf{r}_s$. The net result of collisions and the movement of species in phase space under the influence of external factors define the evolution of the species velocity distribution function throughout time. [Schunk, 1977].

The well-known Boltzmann equation provides a mathematical account of this evolution:

$$\frac{\partial f_s}{\partial \mathrm{t}} + \mathbf{v}_s.\nabla f_s + \left(\frac{e_s}{m_s}\right)\left[\boldsymbol{E} + \frac{\mathbf{v_s}\times\mathbf{B}}{c}\right].\nabla_{v_s} f_s = \frac{\delta f_s}{\delta t} \tag{1}$$

E is the electric field, B is the geomagnetic field, c is the speed of light, ∇ is the coordinate space gradient, and ∇_{v_s} is the velocity space gradient, where e_s and m_s are the charge and mass of species s, respectively. The Boltzmann equation's quantity $\left(\frac{\delta f_s}{\delta t}\right)$ represents the rate at which f_s changes as a result of collisions in a certain area of phase space. The suitable expression for $\left(\frac{\delta f_s}{\delta t}\right)$ for collisions regulated by inverse power potentials and for resonant charge exchange collisions is the Boltzmann collision integral, which is given by

$$\frac{\delta f_s}{\delta t} = \sum_t \int {d_{v_t}}^3 d\Omega\, g_{st}\sigma_{st}(g_{st},\theta)\, [f'_s f'_t - f_s f_t] \tag{2}$$

Where ${d_{v_t}}^3$ is the velocity space volume element of species t, g_{st} is the relative velocity of the colliding particles s and t, $\sigma_{st}(g_{st},\theta)$ is the differential scattering cross section, θ is the scattering angle, $d\Omega$ is the element of solid angle in the s particle reference frame, and the primes denote quantities evaluated after collision.

By solving the Boltzmann equation by the Monte Carlo method Eq.(1) the following distributions were obtained for each ion (In this study, $\mathrm{O}^+$and H^+ ions) the velocity distribution function f_s, density n_s , drift velocity u_s, parallel $T_{s\parallel}$ and perpendicular $T_{s\perp}$ temperatures, and parallel $q_s{}^{\parallel}$and perpendicular $q_s{}^{\perp}$ heat fluxes). The moments considered here, they are defined as follows, which we will use to find the energy of these ions [Barghouthi , 1997]:

$$n_s = \int f_s d\mathbf{v}_s \tag{3}$$

$$u_s = \frac{1}{n_s} \int v_{s\|} f_s d\mathbf{v}_s \tag{4}$$

$$\mathrm{T}_{s\|} = \frac{m_s}{n_s k} \int \left(v_{s\|} - u_s\right)^2 f_s d\mathbf{v}_s \tag{5}$$

$$\mathrm{T}_{s\perp} = \frac{m_s}{2 n_s k} \int (v_{s\perp})^2 f_s d\mathbf{v}_s \tag{6}$$

These Monte Carlo results will be used to calculate the mean parallel energy, mean perpendicular energy, and total mean energy as given in the following expressions [Barghouthi, 1997], respectively:

$$W_{s\|} = \frac{1}{2} m {u_s}^2 + \frac{1}{2} k \mathrm{T}_{s\|} \tag{7}$$

$$W_{s\perp} = k \mathrm{T}_{s\perp} \tag{8}$$

$$W_s = W_{s\|} + W_{s\perp} \tag{9}$$

Where u_s, $\mathrm{T}_{s\|}$ and $\mathrm{T}_{s\perp}$ are given by (4), (5) and (6), respectively and $W_{s\|}$and $W_{s\perp}$are the mean parallel and perpendicular energies, respectively; W_s is the total mean energy; and s denotes the type of the ion ($\mathrm{O}^+$and H^+), k Boltzmann constant.

2.3 Barghouthi Model

Several models, including hydrodynamic, hydromagnetic, generalized transport, kinetic, and semi-kinetic models, were created to predict the behavior of the polar wind plasma. Schunk and Sojka's [1989] provide a detailed analysis of these models and the "classical" descreption of the polar wind. However, because these models can occasionally be confused with one another, it is important to distinguish between the four different varieties. For instance, the kinetic models use collisionless Boltzmann equations to describe both ions and electrons and solve them using the Liouville theorem [e.g., Lemaire and Scherer, 1971]. The plasma developed significant temperature anisotropy ($T_{\parallel} > T_{\perp}$) and an upward heat-flow component as it moves to higher altitudes ($\sim > 5R_E$). Persoon et al. [1983] and Biddle et al. [1985] used observational data to support this traditional description of the arctic wind. Several non-classical features have been introduced throughout the past ten years in order to investigate their impact on plasma outflow. High electron temperature [Barakat and Schunk, 1983] and energetic magnetospheric electrons [Barakat and Schunk, 1984] were discovered to have an impact on the escape flux of O^+, which was shown to be boosted. Barakat et al. [1987] looked into the impact of collisional and chemical H^+-O^+ coupling as well as ion-acceleration at high altitudes on the make-up of the ion escape flux. Recently, a 3-D time-dependent model was created [Schunk and Sojka, 1989], which includes the impact of horizontal drifts on the coupling between the regions above the polar cap, auroral oval, and cusp.

In the models mentioned above, the wave-particle interactions (WPI) were not taken into account. A phenomenological technique was utilized by Ganguli and Palmadesso [1987] and Ganguli et al. [1988] to successfully incorporate the WPI into the generalized transport equations. A number of papers have discussed and developed the Barghouthi model, including Barghouthi and Barakat [1995], Barakat and Barghouthi [1994a,b], Barghouthi [1997, 1998, 2007, 2008], and Barghouthi and Atout [2006]. Barakat and Barghouthi [1994a,b] specifically investigated the impact of WPI on the ion outflow in the polar wind. They included the body force and WPI effects, both of which were demonstrated to be of equivalent significance.

Barghouthi model was developed to study the behavior of ions (H^+ and O^+) outflow at high altitudes and high-latitudes and the simulation results of this model provide a perfect agreements to observations in different regions, auroral region [Barghouthi, 2008] and polar wind region [Barghouthi et al., 2011]. These model simulates different effects which acts on (H^+ and O^+) outflow, the most important of these effects is the wave particle interaction (WPI) (i.e. by using velocity and altitude dependent diffusion coefficient) on H^+ and O^+ outflow in addition to other effects of polarization electrostatic field, gravity and the divergence of the geomagnetic field lines of the planet earth. The main factor underpinning this model is the WPI because it depends on the velocity diffusion coefficient ($D_{\perp}(r, v_{\perp})$), they developed a form for this coefficient as a function of position (r/R_E) along geomagnetic field lines of the Earth and injected ion perpendicular velocity $(v_{\perp})$. The different forms of velocity diffusion coefficient, $D_{\perp}(r, v_{\perp})$ have been used in the Monte Carlo simulation to obtain O^+ and H^+ ions temperatures and velocity distributions at high altitudes in the equatorward region of the cusp. As a result of comparison, we have found an excellent agreement between the observations and the Monte Carlo calculations obtained by Barghouthi model. Also, the results of Barghouthi model for O^+ and H^+ ions distributions and temperatures are consistent with different observations at different altitudes in the auroral region [Barghouthi , 2008].

In the Monte Carlo simulation, the various types of velocity diffusion coefficient, $D_{\perp}(r, v_{\perp})$, were utilized to determine the temperatures and velocity distributions of H^+ and O^+ ions at high altitudes in the equatorward portion of the cusp. We observed that the Monte Carlo simulations produced by the Barghouthi model and the observations had a very good agreement after comparison. Additionally, the Barghouthi model's predictions for the temperatures and ions' distributions in the auroral area are in line with various measurements made at various altitudes.

2.4 Wave Particle Interactions

Ionospheric ions are known to be energetically affected by wave-particle interactions (WPI). This procedure works well over a wide range of altitudes and is crucial in the polar cap, nocturnal oval, and cusp. Ions are heated preferentially in a direction perpendicular to B by the wave-particle interactions, and subsequently they are expelled by the mirror force.

Ionospheric ions that are escaping have energies ranging from 10 eV to 17 keV.[Sharp et al.,1974; Shelley et al.,1982 ; Collin et al.,1987; Horwitz et al.,1992] are a few examples. Wave-particle interactions are most powerful at the dayside cusp, where they energize ionospheric ions to transverse energies between 10 and 50 eV, including (O^+, H^+, He^+, N^+, O^{++}, NO^+, ${O_2}^+$, and ${N_2}^+$). As the heated ions convect in an antisunward direction across the polar cap as a result of magnetospheric electric fields, they are subsequently propelled upward by the gradient-B force. While the more energetic heavy ions escape to the plasma sheet, the lower energy ones fall back to Earth. The final outcome is a phenomenon known as the "cleft ion fountain" [Lockwood et al., 1985].

There have been numerous investigations into how wave-particle interactions affect ion outflow. Because the recorded levels of wave turbulence in this area are several orders of magnitude higher than those detected in the polar cap, the impacts of WPI were initially investigated in this area [Gurnett et al., 1984]. In order to analyze the transverse heating of O^+ caused by a cyclotron resonance with broadband electromagnetic turbulence, Chang et al.[1986] and Retterer et al.[1987a] employed a Monte Carlo code.

It was possible to generate O^+ conics with properties that agreed with the measurements by using an imposed wave spectral density that was constant with height. Ganguli and Palmadesso [1987] and Ganguli et al. [1988] used a phenomenological method to investigate the impact of WPI on field-aligned transport in the auroral return current zone. Their model took into account both the anomalous resistivity (electron heating) and the electrostatic ion cyclotron instability (perpendicular ion heating), and it was based on the 16-moment set of transport equations.

Because the escape of ionospheric ions to the magnetosphere is a crucial ionosphere magnetosphere coupling mechanism, it is crucial to explore the impact of (WPI) on ion out fluxes in the polar wind and aurora regions.

According to Retterer et al. [1987a] illustration, the effects of (WPI) are depicted as particle diffusion in the velocity space.

$$\left.\frac{\delta f}{\delta t}\right|_{WPI} = \left(\frac{1}{v_\perp}\right)\frac{\partial}{\partial v_\perp}\left[D_\perp v_\perp \frac{\partial f}{\partial v_\perp}\right] \tag{10}$$

Where $D_\perp$ is provided by Retterer et al. [1987a] and represents the quasi-linear velocity diffusion rate perpendicular to the geomagnetic field.

$$D_\perp = \frac{q^2}{m^2}\sum_{n=-\infty}^{\infty}\int\frac{d\omega}{2\pi}\int\frac{d^3k}{2\pi^3}\left[\frac{n\Omega}{\omega}\right]^2 A_n \pi\delta\left(\omega - n\Omega - k_\parallel v_\parallel\right) \tag{11}$$

With

$$A_n = \frac{1}{2} {J_{n-1}}^2 |E_L|^2(k,\omega) + \left[\frac{v_{\parallel} {J_n}^2}{v_{\perp}}\right]^2 \left|E_{\parallel}\right|^2(k,\omega) + \frac{1}{2} {J_{n+1}}^2 |E_R|^2(k,\omega) \quad (12)$$

In these equations, q is the ion's charge, m is the ion's mass, Ω is the ion's gyrofrequency, ω is the angular frequency of the electromagnetic turbulence, k is the wave vector.

$J_n = J_n\left(\frac{k_{\perp} v_{\perp}}{\Omega}\right)$, is the standard Bessel function, and $|E_L|^2$ and $|E_R|^2$ are the spectral densities of the electric field in the two perpendicular polarizations. Retterer et al. [1987b] assumed ($k_{\parallel} v_{\parallel} \ll \Omega_i$), $n = 1$ and $(k_{\perp} v_{\perp}/\Omega_i \ll 1)$, and found that

$$D_{\perp} = (\eta\, q^2/4m^2)|E_x(\omega = \Omega)|^2 \quad (13)$$

Where $|E_L(\omega)|^2 = \eta\ |E_x(\omega)|^2$, $|E_x(\omega)|^2$ is the measured spectral density of the electromagnetic turbulence, and η is the proportion of the measured spectral density by plasma wave instrument (PWI) on board the DE-1 spacecraft that corresponds to the left-hand polarized wave.

This equation (13) express for the velocity diffusion rate, $D_{\perp}$ is independent of velocity and depends on position (altitude) via changes in the ion gyrofrequency, Ω, along the geomagnetic field lines.

After analyzing the data gathered by PWI on board the DE-1 spacecraft, Barghouthi [1997] and Barghouthi et al. [1998] produced the following formulas for $D_{\perp}$ in the region equatorward of the cusp.

Many theoretical studies [Chang and Coppi, 1981; Chang et al., 1986; Retterer et al., 1987a, b, 1994; Crew et al., 1990; Barghouthi, 1997, 2008; Barghouthi and Atout, 2006; Bouhram et al., 2003a, b, 2004] concluded that while examining auroral and cusp ion outflows, it is crucial to evaluate the impact of wave particle interactions). Additionally, it was discovered by Barakat and Barghouthi [1994a,b], Barghouthi et al. [1998], Lemaire et al. [2007], and Tam et al. [2007] that wave-particle interactions (WPI) have a significant impact on how ion outflows behave in the polar wind region. The term that represents the interaction between ions and the electromagnetic turbulence, which is resonant interactions at ion gyrofrequency, is substituted for the right-hand side of the Boltzmann equation in order to take the effect of WPI into account in a collisionless region. According to Retterer et al. [1987a], this is represented by the particle diffusion equation in the velocity space:

$$\left[\frac{\delta f_j}{\delta t}\right]_{WPI} = \left(\frac{1}{v_\perp}\right)\frac{\partial}{\partial v_\perp}\left[D_{\perp\,\mathrm{j}}\, v_\perp\, \frac{\partial f_j}{\partial v_\perp}\right] \quad (14)$$

The quasi-linear velocity diffusion coefficient ($D_\perp$) is used. By adding a random increment to the ion's perpendicular velocity ($\Delta v_\perp$), the effect of WPI on the ion during (Δt) is considered, and the ion heating rate as a result of these random increments is consistent with the velocity diffusion coefficient:

$$\langle(\Delta v_\perp)^2\rangle = 4D_\perp \Delta t \quad (15)$$

Where (Δt) denotes the randomly selected time interval, ($D_\perp = (1/2\,m)\ dW_{wave}/dt$) denotes the velocity diffusion coefficient, (dW_{wave}/dt) denotes the rate at which ions are heated by wave particle interaction, and (m) denotes the mass of the ions. It is significant to note that two Gaussian random variables are chosen to represent the two components of $\Delta v_\perp$ in the plane perpendicular to the geomagnetic field lines such as $\langle \Delta v_x{}^2\rangle = \langle \Delta v_y{}^2\rangle = 2D_\perp \Delta t$; the ion's transverse velocity is increased by the vector $\Delta v_\perp$, which is assumed to be randomly oriented with respect to the gyrophase. The time step Δt ought to be zero ($\Delta t \to 0$). However, the computational time grows as Δt decreases, the simulation was run for progressively lower values of Δt until the results were insensitive to the precise value of Δt in order to choose the best value of Δt that strikes a balance between speed and accuracy. The ideal time step was specifically discovered to be $\Delta t \sim 0.01 v_{th}{}^2 / D_\perp$, where v_{th} is the thermal speed of the simulated ion species. This requirement ensures that the average velocity perturbation is significantly smaller than the thermal speed of the ambient ions for each time step. We see that Δt relies on both the kind and the position of the ion.

By examining experimental data of electric field spectral density obtained by PWI onboard the DE-1 satellite (i.e. for high solar activity conditions), Barghouthi [1997] and Barghouthi et al. [1998] calculated the altitude dependence of ($D_\perp$). They came up with the following expressions for the velocity diffusion coefficient $D_\perp$ in the polar wind region [Barghouthi et al., 1998] as follows:

$$D_{\perp}(r) = \begin{Bmatrix} 5.77 \times 10^{3} \left(\frac{r}{\mathrm{R_E}}\right)^{7.95} cm^2 s^{-3}, \text{for } \mathrm{H}^+ \\ 9.55 \times 10^{2} \left(\frac{r}{\mathrm{R_E}}\right)^{13.3} cm^2 s^{-3}, \text{for } \mathrm{O}^+ \end{Bmatrix} \quad (16)$$

In the auroral region, $D_{\perp}(r)$ is given by Barghouthi [1997] as follows:

$$D_{\perp}(r) = \begin{Bmatrix} 4.45 \times 10^{7} \left(\frac{r}{\mathrm{R_E}}\right)^{7.95} cm^2 s^{-3}, \text{for } \mathrm{H}^+ \\ 6.94 \times 10^{5} \left(\frac{r}{\mathrm{R_E}}\right)^{13.3} cm^2 s^{-3}, \text{for } \mathrm{O}^+ \end{Bmatrix} \quad (17)$$

In central polar cap (CPC) and cusp regions, $D_{\perp}(r)$ is given by Nilsson et al. [2013] as follows, respectively;

For central polar cape region

$$D_{\perp}(r) = \begin{Bmatrix} 20 \left(\frac{r}{\mathrm{R_E}}\right)^{9.77} cm^2 s^{-3}, \text{for } \mathrm{H}^+ \\ 0.5 \times 10^{5} \left(\frac{r}{\mathrm{R_E}}\right)^{5.5} cm^2 s^{-3}, \text{for } \mathrm{O}^+ \end{Bmatrix} \quad (18)$$

And for cusp region

$$D_{\perp}(r) = \begin{Bmatrix} 1.01 \times 10^{6} \left(\frac{r}{\mathrm{R_E}}\right)^{5.61} cm^2 s^{-3}, \text{for } \mathrm{H}^+ \\ 2.5 \times 10^{4} \left(\frac{r}{\mathrm{R_E}}\right)^{6.4} cm^2 s^{-3}, \text{for } \mathrm{O}^+ \end{Bmatrix} \quad (19)$$

The diffusion coefficient was given a new form by Barghouthi [2008], who discovered that it is a velocity-dependent in addition to altitude-dependent.

$$D_{\perp}(r, v_{\perp}) = D_{\perp}(r) \begin{Bmatrix} 1 & \text{for } \left(\frac{k_{\perp} v_{\perp}}{\Omega_i}\right) < 1 \\ \left(\frac{k_{\perp} v_{\perp}}{\Omega_i}\right)^{-3} & \text{for } \left(\frac{k_{\perp} v_{\perp}}{\Omega_i}\right) \geq 1 \end{Bmatrix} \quad (20)$$

Where $D_{\perp}(r, v_{\perp})$ is the quasi-linear velocity diffusion rate perpendicular to the geomagnetic field lines (altitude and velocity dependent) , Ω_i is the ion gyrofrequency and $k_{\perp}$ is perpendicular wave number and related to the characteristic perpendicular wavelength of the electromagnetic turbulence $\lambda_{\perp}$.

According to Eq. (20), we plot the relationship between the diffusion coefficient and the altitudes in each of the polar wind and aurora regions based on the information given by Nilsson et al., [2013] and how will the diffusion coefficient values change when it starts to depend on velocity as well, for example, as seen in Figure 2.2, The diffusion coefficient values begin to increase with altitude without any effect, i.e. the diffusion coefficient still depends on altitude only (blue solid line), ($\left(\frac{k_\perp v_\perp}{\Omega_i}\right)$ is less than 1) in Figure 2.2 (left) in auroral region and Figure 2.2 (right) in polar wind region for O^+ ions , but after certain altitudes $2R_E$ and $3R_E$ for aurora and polar wind regions respectively , the values of diffusion coefficient begin to be decreasing by amount $\left(\frac{k_\perp v_\perp}{\Omega_i}\right)^{-3}$ (blue dashed line) , that means $\left(\frac{k_\perp v_\perp}{\Omega_i}\right)$ is greater than 1 and the diffusion coefficient become also velocity dependent. All these changes will appear clearly when calculating energy in the coming sections.

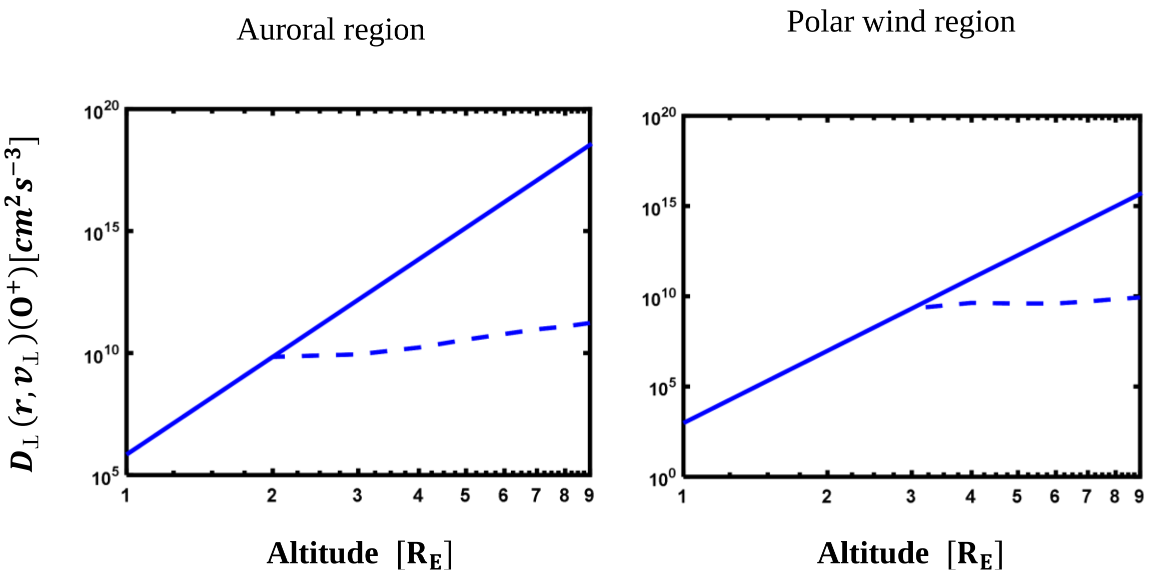

Figure 2.2. Altitude profiles of the diffusion coefficients in auroral region (left) and polar wind region (right) for O^+ ions, where the (blue solid line) represents the altitude dependent diffusion coefficient, and (blue dashed line) represents the altitude and velocity diffusion coefficient for electromagnetic wavelength $\lambda_\perp = 8\ km$.

2.5 Ion Heating

Each ion is first powered by a specific electromagnetic ion cyclotron (EMIC) wave whose Doppler-shifted frequency, caused by $k_\parallel v_\parallel$ locally matches the ion's gyrofrequency. The magnetic field's mirror geometry converts some of the ion's transverse energy into parallel energy as it gains energy, which causes the ion to begin drifting upward along the magnetic field lines. As long as the local wave intensity stays reasonably strong, significant heating through this broad band resonance process continues of the order of $10^{-8} - 10^{-6}\ \mathrm{V^2/m^2}$ Hz or a few $\mathrm{mV/m}$ in total field strength over the entire low frequency range in our present application [Chang et al.,1986].

For an ensemble of gyrotropically dispersed ions in a fluctuating magnetic field, Chang et al. [1986] provided below a heuristic derivation of an EMIC resonance heating formula. Using more rigorous quasilinear arguments, this result (which is comparable to Eldrige's finding from 1972 for electron heating in mirror machines) can be reached [Sagdeev and Galeev, 1969]. Because the heuristic derivation involves extremely basic physics principles and concepts that are appealing to the human mind, here is the derivation.

Consider a generic ion that is subject to a broad band of EMIC waves and is located in an ambient magnetic field B. The ion will only interact with the specific EMIC wave whose Doppler shifted frequency owing to $k_{\|}v_{\|}$ matches the ion's gyrofrequency $f_{ci} = \frac{qB}{2\pi mc}$,where q and m are the ion's charge and mass, respectively. In time intervals longer than the ion gyroperiod, only resonant waves will result in a net heating of the ion. For resonant interaction, the net increase of the perpendicular component of the velocity vector $v_{\perp}$ of the ion in time Δt is $\Delta v_{\perp}$ = $(\frac{qE_{\perp}}{m})\Delta t$, where $E_{\perp}$ is the perpendicular component of the wave electric filed vector in the polarization mode which can resonate with ion species (for example, the left-hand polarized component in the case of positive ions). (The oscillating magnetic field has almost no impact on particle acceleration application [Chang et al.,1986]

. Thus the net increase in the perpendicular energy of the ion in time Δt is

$$\Delta W_{\perp} = \frac{1}{2}m(v_{\perp} + \Delta v_{\perp})^2 - \frac{1}{2}m{v_{\perp}}^2 = mv_{\perp}.\Delta v_{\perp} + \frac{1}{2}m(\Delta v_{\perp})^2 \qquad (21)$$

Now that the group of identical ions is gyrotropically distributed, we will discover that there is a second ion with a perpendicular component of velocity equal to -$v_{\perp}$ for each generic ion. The first part in Eq. (21) in the right side balances out for the two ions, and each ion in the generic pair of ions experiences a net incremental rise in $W_{\perp}$ that is equal to

$$\Delta W_{\perp,\mathrm{res}} = \frac{1}{2}\frac{(qE_{\perp})^2}{m}(\Delta t)^2 \tag{22}$$

We define ${E_{\perp}}^2 = \sum(f_{ci}(l), l)\Delta f,$ where Δf is some bandwidth and $\sum(f, l)$ is the wave electric field spectral density. In order to obtain an estimate of the net heating rate per ion, we can rearrange Eq.(22). The actual spectrum is smooth enough close to the local ion gyrofrecquancy, and the Doppler shift caused by $k_{\|}v_{\|}$ is modest enough to be ignored when calculating $\sum$.

$$\dot{W}_{\perp,\mathrm{res}} = q^2 \sum(f_{ci}(l), l)\Delta f\, \Delta t/2m \tag{23}$$

where the time difference is indicated by a dot. The correlation time of the incoherent electric field at frequencies close to the local gyrofrequncy limits the resonance time in our application because the actual spectrum is sufficiently broad in frequency. As a result, we employ the well-known relation $\Delta f \Delta t \approx 1$.

$$\dot{W}_{\perp,\mathrm{res}} \approx q^2 \sum(f_{ci}(l), l)/2m \tag{24}$$

The ion loses resonance with the first band of EMIC waves with frequencies Δf around $f_{ci}(l)$ as it moves down the geomagnetic field line from l to $'$ and gains resonance with a second band of EMIC waves with frequencies $\Delta f'$ around its new gyrofrequncy $f_{ci}(l')$.In light of this, statement (24) continues to be true as the ion rises along the filed line.

2.6 Mean Particle Theory (MPT)

Chang et al.[1986] provided a theory for estimation of the values of the mean perpendicular, mean parallel, and mean total energies as a function of geocentric distance by including the average rate of heating for each ion in a set of equations that describe the motion of the ion along geomagnetic field lines, as follows,

$$W_{i\|} = \frac{9m_i}{2^{1/3}}\left[\frac{rD_{\perp}(r)}{(3\alpha+1)(6\alpha+11)}\right]^{2/3} \tag{25}$$

$$W_{i\perp} = \frac{(6\alpha+2)m_i}{2^{1/3}}\left[\frac{rD_{\perp}(r)}{(3\alpha+1)(6\alpha+11)}\right]^{2/3} \tag{26}$$

$$W_i = \quad W_{i\|} + W_{i\perp} = (3\alpha + 11/2)^{1/3} m_i \left[\frac{rD_{\perp}(r)}{(3\alpha+1)}\right]^{2/3} \tag{27}$$

Where $W_{||}$ and $W_{\perp}$ are the mean parallel and perpendicular energies, respectively; W_i is the total mean energy; and i denotes the type of the ion (H^+ or O^+). In that theory the mean energy ratio $W_{\perp}/W_{||}$ asymptotically approaches a constant value.

2.6.1 Mean particle calculations

An ion's unaltered orbit can be followed along the geomagnetic field line in the absence of broad band EMIC (Electromagnetic Ion Cyclotron) resonance heating. Increases in perpendicular energy occur as a result of EMIC heating at a rate of $\dot{W}_{\perp,res}$. Eq. (24) can be used to get the average rate of resonant heating in a particle computation for gyrrotropically distributed ions. Using the guiding center approximation, the evolution equations for a mean particle can thus be expressed as

$$\dot{W}_{\perp} = W_{\perp} v_{||}\, dlnB/dl + \dot{W}_{\perp,\mathrm{res}} \qquad (28)$$

$$m\dot{v}_{||} = qE_{||} - W_{\perp}\, dlnB/dl \qquad (29)$$

Where $E_{||}$ is the filed-aligned electric field and $v_{||} = dl/dt$ is the parallel component of the mean particle's velocity. The previously derived Eqs. (28,29) for broad band, lower hybrid heating [Chang and Coppi,1981] are comparable. Naturally, EMIC waves rather than lower hybrid waves are now to blame for the heating.

The observed low frequency electric filed energy density spectra in the CPS, may be approximately represented by

$$\Sigma(f) = \Sigma_0 (f_0/f)^{\alpha} \qquad (30)$$

Where α is a fitting parameter and $\Sigma_0 = \Sigma(f_0)$ and $f_0 = f_{ci}(l_0)$, the ion gyrofrequency at some reference geocentric altitude l_0.

In the absence of Electromagnetic Ion Cyclotron, and the ion moved a distance dx in an interval of time dt, $W_{i\perp}$ is decreased by :

$$dW_{i\perp} = W_{i\perp} dx_{\parallel} \frac{\partial lnB}{\partial x_{\parallel}} \quad , \; dx_{\parallel} = v_{i\parallel}\, dt$$

Derivation

$$\frac{1}{W_{i\perp}} \frac{dW_{i\perp}}{dx_{\parallel}} = \frac{1}{B} \frac{\partial B}{\partial x_{\parallel}}$$

$$dW_{i\perp} = W_{i\perp} dx_{\parallel} * \frac{\partial lnB}{\partial x_{\parallel}}$$

$$dW_{i\perp} = W_{i\perp} v_{i\parallel}\, dt * \frac{\partial lnB}{\partial x_{\parallel}} \quad \Longrightarrow \quad \boxed{\dot{W}_{i\perp} = W_{i\perp}\, v_{i\parallel} \frac{\partial lnB}{\partial x_{\parallel}}}$$

$$\frac{dW_{i\perp}}{dt} = W_{i\perp} v_{i\parallel} \frac{\partial lnB}{\partial x_{\parallel}}$$

$$\dot{W}_{\perp} = W_{\perp} v_{\parallel} \frac{\partial lnB}{\partial l} + 2mD_{\perp} \quad , \; m\dot{v}_{\parallel} = -W_{\perp} \frac{\partial lnB}{\partial l}$$

$$m v_{\parallel} \dot{v}_{\parallel} = -W_{\perp} v_{\parallel} \frac{\partial lnB}{\partial l}$$

$$\frac{d\left(\frac{1}{2} m v_{\parallel}{}^{2}\right)}{dt} = -W_{\perp} v_{\parallel} \frac{\partial lnB}{\partial l} \quad \Longrightarrow \quad \boxed{\frac{\mathrm{d}\left(W_{\parallel} + W_{\perp}\right)}{\mathrm{dt}} = 2mD_{\perp}}$$

For upward motion

$$F = m\dot{v}_{\parallel} = qE_{\parallel} - \mu \frac{\partial B}{\partial x_{\parallel}} \qquad , \; F = m\dot{v}_{\parallel} = qE_{\parallel} - \frac{W_{\perp}}{B} \frac{\partial B}{\partial x_{\parallel}}$$

$$F = m\dot{v}_{\parallel} = qE_{\parallel} - W_{\perp} \frac{\partial lnB}{\partial x_{\parallel}}$$

$$\boldsymbol{\frac{dW}{dt} = 2mD_{\perp}}$$

$$m\dot{v}_{\parallel} = -W_{\perp} \frac{\partial lnB}{\partial l} \qquad , \qquad \dot{W}_{\perp} = W_{\perp} v_{\parallel} \frac{\partial lnB}{\partial l} + \frac{q^{2}}{2m} E_{0} \left(\frac{f_{0}}{f}\right)^{\alpha}$$

$$\dot{W}_{\perp} = -v_{\parallel}\left[m\dot{v}_{\parallel}\right] + \frac{q^{2}}{2m} E_{0} \left(\frac{f_{0}}{f}\right)^{\alpha} \qquad , \qquad \dot{W}_{\perp} = -\, m v_{\parallel} \dot{v}_{\parallel} + 2mD_{\perp}$$

$$\frac{d(W_{\perp})}{dt} + \frac{d\left(\frac{1}{2} m v_{\parallel}{}^{2}\right)}{dt} = 2mD_{\perp} \quad \Longrightarrow \quad \boxed{\frac{dW}{dt} = 2mD_{\perp}}$$

$$\frac{dW}{dt} = 2mD_{\perp} = \frac{2mq^{2}}{4m^{2}} \sum_{0} (f_{0}/f)^{\alpha} = \frac{2mq^{2}}{4m^{2}} \sum_{0} f_{0}{}^{\alpha} \left(\frac{m}{qB}\right)^{\alpha} = \frac{2mq^{2}}{4m^{2}} \sum_{0} f_{0}{}^{\alpha} \left(\frac{m}{qB_{0}}\right)^{\alpha} l^{3\alpha}$$

Let $\boldsymbol{\frac{dW}{dt} = cl^{3\alpha}}$

$$\mathrm{dt} = \frac{dl}{v_\parallel} \qquad then\ \ v_\parallel \frac{dW}{dl} = cl^{3\alpha} \ \rightarrow\rightarrow v_\parallel = c'v = cW^{1/2}$$

$$\mathrm{c'W^{1/2}}dW = cl^{3\alpha}dl \ \rightarrow\rightarrow W^{3/2} = Cl^{3\alpha+1} \rightarrow\rightarrow W = cl^{(3\alpha+1)\frac{2}{3}} = cl^{2\alpha+\frac{2}{3}}$$

$$\boxed{W = cl^{2\alpha+\frac{2}{3}} \ , \quad W_\perp = c_\perp l^{2\alpha+\frac{2}{3}} \qquad , W_\parallel = c_\parallel l^{2\alpha+\frac{2}{3}}}$$

$$\frac{1}{2}m{v_\parallel}^2 = c_\parallel l^{2\alpha+\frac{2}{3}} \rightarrow\rightarrow v_\parallel = \sqrt{\frac{2c_\parallel}{m}}\, l^{\alpha+\frac{1}{3}}$$

$$m\dot{v}_\parallel = -W_\perp \frac{dlnB}{dl} \tag{28}$$

$$\dot{\mathrm{W}}_\perp = \mathrm{W}_\perp v_\parallel \frac{dlnB}{dl} + 2mD_\perp \tag{29}$$

$$\dot{\boldsymbol{v}}_\parallel = \frac{dv_\parallel}{dt} = \frac{dv_\parallel}{\frac{dl}{v_\parallel}} = v_\parallel \frac{dv_\parallel}{dl} \qquad , \qquad \dot{\mathbf{W}}_\perp = \frac{d\mathrm{W}_\perp}{dt} = \frac{d\mathrm{W}_\perp}{\frac{dl}{v_\parallel}} = v_\parallel \frac{d\mathrm{W}_\perp}{dl}$$

$$\boldsymbol{\frac{dlnB}{dl}} = \left(\frac{\boldsymbol{-3}}{\boldsymbol{l}}\right)$$

$$mv_\parallel \frac{dv_\parallel}{dl} = -\mathrm{W}_\perp \frac{dlnB}{dl} = -\mathrm{W}_\perp \left(\frac{-3}{l}\right) \tag{30}$$

$$v_\parallel \frac{d\mathrm{W}_\perp}{dl} = \mathrm{W}_\perp v_\parallel \left(\frac{-3}{l}\right) + 2mD_\perp \tag{31}$$

$$m\sqrt{\frac{2c_\parallel}{m}}\, l^{\alpha+\frac{1}{3}} \sqrt{\frac{2c_\parallel}{m}} \left(\alpha + \frac{1}{3}\right) l^{\alpha+\frac{1}{3}-1} = -c_\perp l^{2\alpha+\frac{2}{3}} \left(\frac{-3}{l}\right)$$

$$m\frac{2c_\parallel}{m}\left(\alpha + \frac{1}{3}\right) l^{2\alpha-\frac{1}{3}} = 3c_\perp l^{2\alpha-\frac{1}{3}} \rightarrow\rightarrow c_\perp = \frac{2}{3}\left(\alpha + \frac{1}{3}\right) c_\parallel = \left(\frac{2\alpha}{3} + \frac{2}{3}\right) c_\parallel = \left(\frac{6\alpha + 2}{9}\right) c_\parallel$$

$$\boldsymbol{c_\perp = \left(\frac{6\alpha+2}{9}\right) c_\parallel} \qquad \Longrightarrow \qquad \boldsymbol{\frac{W_\perp}{W_\parallel} = \left(\frac{6\alpha+2}{9}\right)}$$

$$v_{\parallel}\frac{dW_{\perp}}{dl} = W_{\perp}v_{\parallel}\frac{dlnB}{dl} + 2mD_{\perp}$$

$$\sqrt{\frac{2c_{\parallel}}{m}}l^{\alpha+\frac{1}{3}}c_{\perp}\left(2\alpha+\frac{2}{3}\right)l^{2\alpha+\frac{2}{3}-1} = c_{\perp}l^{2\alpha+\frac{2}{3}}\sqrt{\frac{2c_{\parallel}}{m}}l^{\alpha+\frac{1}{3}}\left(\frac{-3}{l}\right) + 2mD_{\perp}$$

$$\sqrt{\frac{2c_{\parallel}}{m}}c_{\perp}\left(2\alpha+\frac{2}{3}\right)l^{3\alpha} = -3\sqrt{\frac{2c_{\parallel}}{m}}c_{\perp}l^{3\alpha} + 2mD_{\perp} \rightarrow\rightarrow \sqrt{\frac{2c_{\parallel}}{m}}c_{\perp}l^{3\alpha}\left[2\alpha+\frac{2}{3}+3\right] = 2mD_{\perp}$$

$$\sqrt{\frac{2c_{\parallel}}{m}}\left(\frac{6\alpha+2}{9}\right)c_{\parallel}l^{3\alpha}\left(\frac{6\alpha+11}{3}\right) = 2mD_{\perp} \rightarrow\rightarrow c_{\parallel}{}^{3/2} = \frac{2mD_{\perp}l^{-3\alpha}}{\sqrt{\frac{2}{m}}\left(\frac{6\alpha+2}{9}\right)\left(\frac{6\alpha+11}{3}\right)}$$

$$c_{\parallel} = \left[\frac{2mD_{\perp}l^{-3\alpha}}{\sqrt{\frac{2}{m}}\left(\frac{6\alpha+2}{9}\right)\left(\frac{6\alpha+11}{3}\right)}\right]^{2/3} = m\left[\frac{27\sqrt{2}\,D_{\perp}l^{-3\alpha}}{(6\alpha+2)(6\alpha+11)}\right]$$

$$c_{\parallel} = m\left[\frac{27\,D_{\perp}l^{-3\alpha}}{\sqrt{2}\,(3\alpha+1)(6\alpha+11)}\right]^{2/3} = \frac{9m}{2^{1/3}}\left[\frac{D_{\perp}l^{-3\alpha}}{(3\alpha+1)(6\alpha+11)}\right]^{2/3}$$

$$W(l) = W_{\perp} + W_{\parallel} = c_{\perp}l^{2\alpha+\frac{2}{3}} + c_{\parallel}l^{2\alpha+\frac{2}{3}}$$

$$W(l) = l^{2\alpha+\frac{2}{3}}c_{\parallel}\left[\frac{6\alpha+2}{9}+1\right] = l^{2\alpha+\frac{2}{3}}c_{\parallel}\left[\frac{6\alpha+2+9}{9}\right] \rightarrow W(l)$$
$$= c_{\parallel}\left[\frac{6\alpha+11}{9}\right]l^{2\alpha+\frac{2}{3}}$$

$$W(l) = \frac{9m}{2^{1/3}}\left[\frac{D_{\perp}l^{-3\alpha}}{(3\alpha+1)(6\alpha+11)}\right]^{2/3} l^{2\alpha+\frac{2}{3}}\left(\frac{6\alpha+11}{9}\right)$$

$$W(l) = \frac{m}{2^{1/3}}\left[\frac{D_{\perp}l}{(3\alpha+1)}\right]^{2/3}\frac{(6\alpha+11)}{(6\alpha+11)^{2/3}} = \left(\frac{6\alpha+11}{2}\right)^{1/3} m\left[\frac{D_{\perp}l}{(3\alpha+1)}\right]^{2/3}$$

$$\boldsymbol{W(l) = \left(3\alpha+\frac{11}{2}\right)^{1/3} m\left[\frac{D_{\perp}l}{(3\alpha+1)}\right]^{2/3}} \qquad \textbf{this is Eq. (27), where } \boldsymbol{l = r}$$

$$\boldsymbol{W(l)} = \left(\boldsymbol{3\alpha + \frac{11}{2}}\right)^{1/3} \boldsymbol{m}\left[\frac{\boldsymbol{D_{\perp} l}}{\boldsymbol{(3\alpha+1)}}\right]^{2/3} = \boldsymbol{W_{\parallel} + W_{\perp} = W}$$

And $\quad \dfrac{\boldsymbol{W_{\perp}}}{\boldsymbol{W_{\parallel}}} = \left(\dfrac{\boldsymbol{6\alpha+2}}{\boldsymbol{9}}\right)$ $\quad$ **then** $\quad \boldsymbol{W_{\perp}} = \left(\dfrac{\boldsymbol{6\alpha+2}}{\boldsymbol{9}}\right)\boldsymbol{W_{\parallel}}$

$$W_{\parallel} + W_{\perp} = \left(\frac{6\alpha+2}{9}\right) W_{\parallel} + W_{\parallel} = \left(3\alpha + \frac{11}{2}\right)^{1/3} m\left[\frac{D_{\perp} l}{(3\alpha+1)}\right]^{2/3}$$

$$W_{\parallel}\left(\frac{6\alpha+2}{9} + 1\right) = \left(3\alpha + \frac{11}{2}\right)^{1/3} m\left[\frac{D_{\perp} l}{(3\alpha+1)}\right]^{2/3}$$

$$W_{\parallel}\left(\frac{6\alpha+11}{9}\right) = \frac{(6\alpha+11)^{1/3}}{2^{1/3}} m\left[\frac{D_{\perp} l}{(3\alpha+1)}\right]^{2/3}$$

$$W_{\parallel} = \frac{\frac{(6\alpha+11)^{1/3}}{2^{1/3}}}{\left(\frac{6\alpha+11}{9}\right)}\left[\frac{D_{\perp} l}{(3\alpha+1)}\right]^{2/3} = \frac{(6\alpha+11)^{1/3} 9m}{(6\alpha+11)2^{1/3}}\left[\frac{D_{\perp} l}{(3\alpha+1)}\right]^{2/3}$$

$$W_{\parallel} = \frac{9m}{(6\alpha+11)^{2/3} 2^{1/3}}\left[\frac{D_{\perp} l}{(3\alpha+1)}\right]^{2/3} = \frac{9m}{2^{1/3}}\left[\frac{D_{\perp}(l) l}{(3\alpha+1)(6\alpha+11)}\right]^{2/3}$$

$$\boldsymbol{W_{\parallel}} = \frac{\boldsymbol{9m_i}}{\boldsymbol{2^{1/3}}}\left[\frac{\boldsymbol{D_{\perp}(l) l}}{\boldsymbol{(3\alpha+1)(6\alpha+11)}}\right]^{2/3} \qquad \textbf{this is Eq. (25) in general}$$

$$W_{\perp} = \left(\frac{6\alpha+2}{9}\right) W_{\parallel} = \left(\frac{6\alpha+2}{9}\right)\frac{9m}{2^{1/3}}\left[\frac{D_{\perp}(l) l}{(3\alpha+1)(6\alpha+11)}\right]^{2/3}$$

$$\boldsymbol{W_{\perp}} = \frac{\boldsymbol{(6\alpha+2)m_i}}{\boldsymbol{2^{1/3}}}\left[\frac{\boldsymbol{D_{\perp}(l) l}}{\boldsymbol{(3\alpha+1)(6\alpha+11)}}\right]^{2/3} \qquad \textbf{this is Eq. (26)in general}$$

CHPETER THREE

RESULTS AND DISCUSSIONS

3.1 Introduction

Initially, we will provide and discuss many comparisons between the Monte Carlo method simulations and the estimates of the mean particle theory in different regions and under different conditions, as shown in the following sections. Later in section 3.5 we will compare between Monte Carlo simulations, estimates of mean particle theory, and available observations.

3.2 Comparison between Monte Carlo simulations and estimates of Mean Particle Theory

In this section we present comparisons between estimates of the values of the mean perpendicular, parallel, and total energies as a function of geocentric distance with including the mean heating rate per ion in a set of equations which describe the motion of an ion-guiding center along the geomagnetic field lines, here we considered the diffusion coefficient to be altitude dependent and not velocity dependent, with Monte Carlo simulations These comparisons obtained in the auroarl, polar wind, central polar cap, and cusp regions.

3.2.a Auroral Region

We have obtained altitude profiles for ion drift velocity, parallel temperature, and perpendicular temperature by using Barghouthi model [Barghouthi, 2008], i.e. equations 4, 5, and 6, and by using these results we have calculated the mean parallel, perpendicular and total energies (equations 7, 8, and 9) for both ions O^+ and H^+ in the altitude range from 1.7 $\mathrm{R_E}$ to 9 $\mathrm{R_E}$. The estimates of the mean particle theory are obtained by using Eqs. (25), (26), and (27), in these equations we have considered the diffusion coefficients $D_\perp(\mathrm{O}^+)$ and $D_\perp(\mathrm{H}^+))$ to be altitude dependent only. The differences between the behavior of the O^+ and H^+ ions are due to the large mass ratio $\mathrm{m}(\mathrm{O}^+) = 16\mathrm{m}(\mathrm{H}^+)$ and perpendicular diffusion coefficient, where

$D_\perp$ (O^+) larger than $D_\perp$ (H^+). Figure 3.1 shows the outcome of our comparisons, O^+ ions (right) and H^+ ions (left) and the results of our calculations for the mean perpendicular energy $W_\perp$ (panels a and d), mean parallel energy $W_{||}$(panels b and e) and total energy W_{total} (panels c and f). The estimates of the mean particle theory (blue solid lines) and Monte Carlo simulations (red dashed lines). Figure 3.1 (right), which compares the two methods, demonstrates great agreement in the case of O^+ ions. For instance, in the case of $W_\perp$ and $W_{||}$, it is impossible to tell the difference between the Monte Carlo and the estimations of the mean particle theory . H^+ ion profiles are compared in Figure 3.1 (left). At altitudes greater than $3R_E$, there is excellent agreement between the Monte Carlo results and the mean particle theory estimates, but the variations in the results at lower altitudes are simply explained by the asymptotic approximation in the mean particle formulas. For instance, the conclusions of the mean particle theory $W_\perp$ and $W_{||}$ approach zero as r approaches zero, as seen in Figure 3.1. In addition, the mean particle hypothesis holds true at altitudes where the ion's realized energies are significantly greater than the distribution's beginning energies, indicating that the distribution's initial state has been forgotten Retterer et al.[1987a]. Also as we have seen the total energy for both H^+ and O^+ ions are in excellent agreement by two methods at high altitudes with small differences at low altitudes.

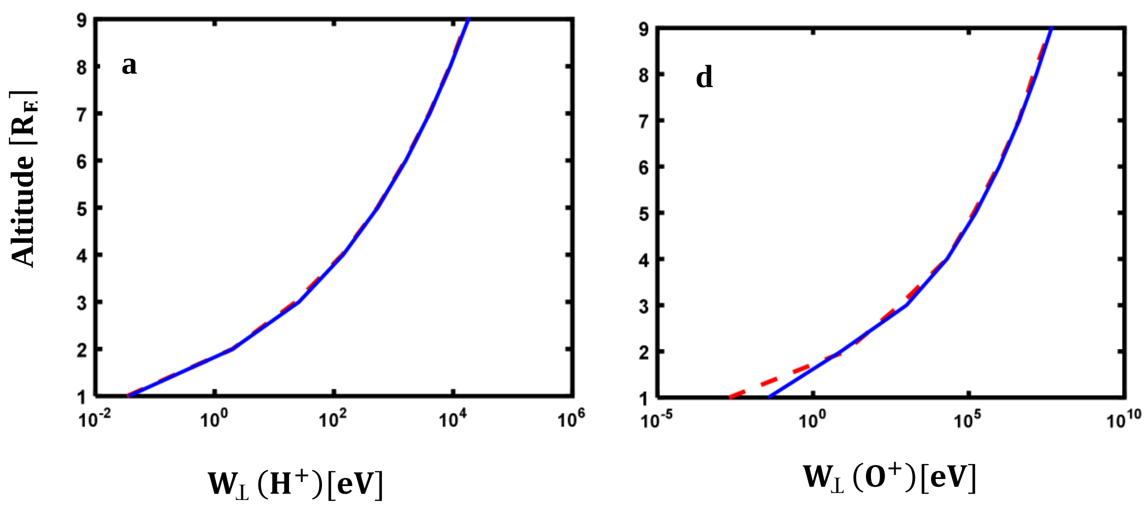

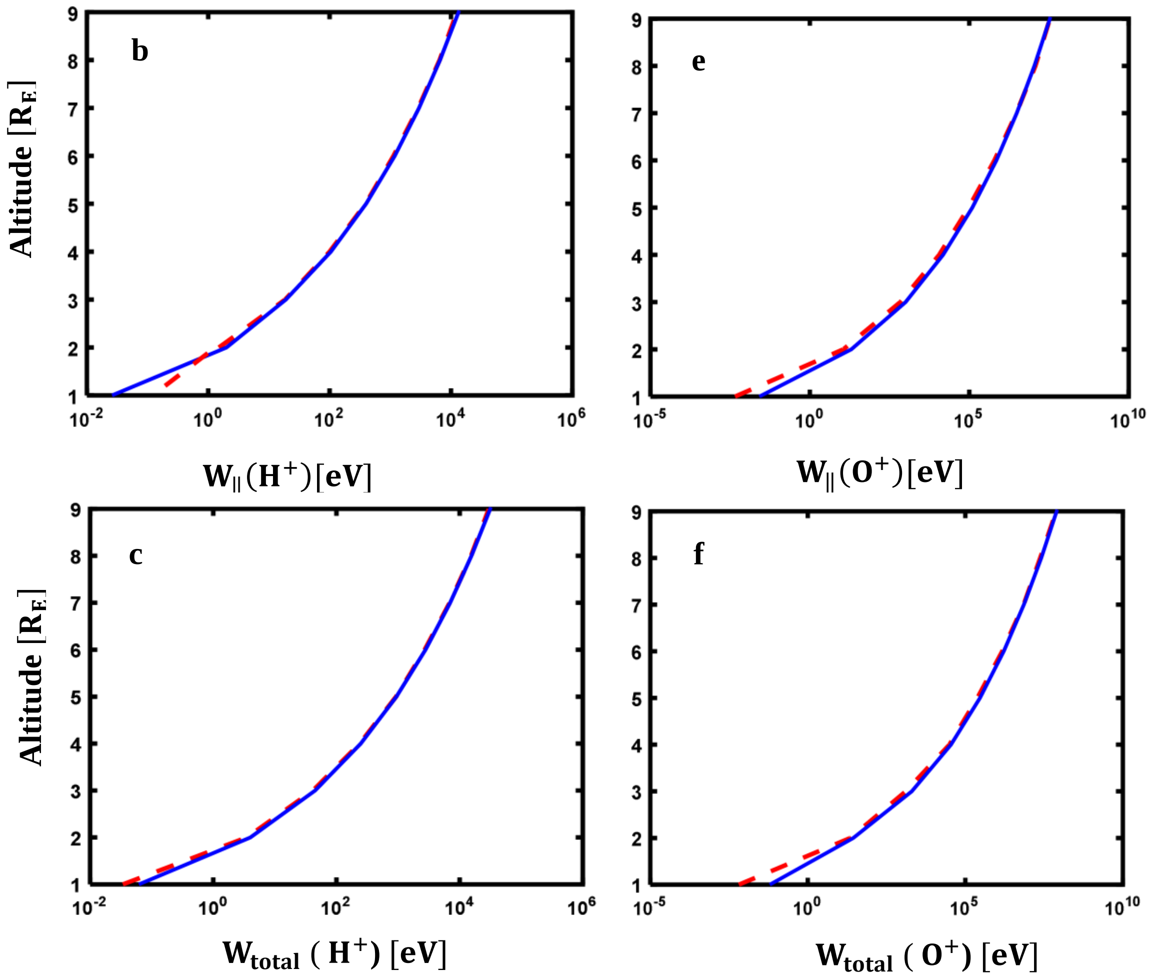

Figure 3.1. Altitude profiles of the estimates of the mean particle theory (blue solid lines) for auroral conditions with the Monte Carlo calculations (red dashed lines). Left panels, a, b, and c are for H^+ ions. Right panels, d, e, and f are for O^+ ions. The mean perpendicular energy W_L considered here (panels a and d), mean parallel energy $W_{||}$ (panels b and e) and mean total energy W_{total} (panels c and f).

Given this, predictions of the mean particle theory at low altitudes differ from those of Monte Carlo, revealing higher levels for H^+ than for O^+. This difference is most likely caused by the beginning circumstances for O^+ being expected to be closer to those predicted by the mean particle theory at the injection altitude. As a result, O^+ ions quickly acquired sufficient energy as a result of WPI and entered the asymptotic domain. At lower altitudes, however, the beginning circumstances for H^+ are very different from what the mean particle theory predicts. H^+ ions must therefore drift to a greater altitude in order to gain sufficient energy through WPI to enter the asymptotic regime.

3.2.b Polar Wind Region

Similarly, in the polar wind region, we have investigated the variation of energies with ascent to higher altitudes, but the situation is slightly different from the auroral region due to the initial conditions and altitude profiles of the different O^+ and H^+ moments, ion density, drift velocity, parallel temperature, and perpendicular temperature obtained by Barghouthi et al. [2011]. Barghouthi model has been applied by using beginning circumstances and velocity diffusion coefficients appropriate for the polar wind region, the auroral region can likewise be described by the model; the only differences are the border conditions that represent the region and the diffusion coefficient's altitude dependency (i.e. $D_{\perp}$ (r)). Barghouthi et al. [2011] displayed the O^+ ion velocity distribution function f (O^+) and H^+ ions velocity distribution functions f (H^+) at various elevations in the simulation tube with altitude profiles of the lower order O^+ and H^+ moment at various values of characteristic wavelengths for the electromagnetic turbulence ($\lambda_{\perp} = \infty, 50, 20, 8,$ and 1 km). In this part, we have taken one of these cases when the wavelengths for the electromagnetic turbulence turn into infinity ($\lambda_{\perp} = \infty$) , while the rest will be discussed in the following sections.

According to Eq.(6) the expression of the diffusion coefficient ($D_{\perp}$) varies with the change in the values of the $\lambda_{\perp} = \infty$ from being dependent on the altitude to dependent also on the velocity and the case that we are interested in is ($\lambda_{\perp} \rightarrow \infty$) i.e. $k_{\perp} \rightarrow 0$. The altitude profiles for O^+ and H^+ moments were presented separately in Barghouthi et al.[2011] from 1.7 R_E to 13.7 R_E and the behaviors of these moments ($n_i, u_i, T_{i\perp}$ and $T_{i\parallel}$) when ($\lambda_{\perp} \rightarrow \infty$) , this data will be used to obtain ($W_{\perp}$, $W_{\parallel}$ and W_{total}) from 1.7 R_E to 10 R_E . We have used the appropriate altitude dependent diffusion coefficient in the polar wind and obtained the estimates of the mean particle theory, i.e. Eqs. (25), (26), and (27).

Figure 3.2 shows the comparative results which presents the outflow of H^+ ions (left) and O^+ ions (right). We started our calculations by mean particle theory (blue solid lines) for mean perpendicular energy $W_{\perp}$ (panels a and d) where the increase appears clearly with increasing altitudes and smoothly from 1.7 R_E to 9R_E for both H^+ and O^+ ions with $W_{\perp}(O^+) > W_{\perp}(H^+)$, this is due to difference in perpendicular diffusion coefficient and the mass of each of them. At the same time the results of the Monte Carlo calculations were represented (red dashed lines) at the same figure the behavior of perpendicular energy depends on the behavior of $T_{\perp}(H^{+})$, whereas the energy starts to drop from 1.7 R_E to 5 R_E and at altitudes greater than 5 R_E is monotonously growing. As well as the perpendicular energy depends on $T_{\perp}(O^{+})$ behavior which rises as a result of the influence of WPI, which due to the influence of perpendicular adiabatic cooling. As a result of the comparison between the two methods it is clear there is a difference between mean particle theory and the Monte Carlo calculations behaviors with altitudes.

For the mean parallel energy $W_{||}$ (panels b and e) also the behavior by mean particle theory is increasing consistently and smoothly with altitudes for both H^{+} and O^{+} ions but in Monte Carlo behavior for H^{+} ions, we note that there is an intersection with the mean particle theory behavior at 4 R_E , then both curves continue to increase with a significant difference between them at high altitudes, this is because the mean parallel energy values $W_{||}(H^{+})$ in Monte Carlo method depend on both (parallel temperature $T_{||}(H^{+})$ which increasing at high altitudes ~ 9.39 R_E and decreases at lower altitudes and drift velocity $u(H^{+})$ which increases with altitude) as described in Barghouthi et al.[2011] , in contrast for mean parallel energy of O^{+}ions $W_{||}$ (O^{+}) it is very good result, the values are close to each other in both ways, and there is a convergence in the two behaviors due to ($T_{||}(O^{+})$ at high altitudes increasing above ~ 4.27 R_E and falls below this altitude and $u(O^{+})$ increasing rapidly) as described by Barakat and Lemaire [1990]. We are also interested to compare the total energy W_{total} (panels c and f), we calculated the total energy, it is clear that the W_{total} by using the mean particle theory takes the same form for both mean parallel energy and mean perpendicular energy it is increasing smoothly and rapidly in both O^{+} and H^{+} ions while in Monte Carlo calculations behavior appeared slightly different and there is divergence between the two curves for both O^{+} and H^{+} ions. To be specific, in polar wind region we have qualitative agreement, behavior, but poor quantitative agreement for O^{+} ions, and no agreement for H^{+} ions.

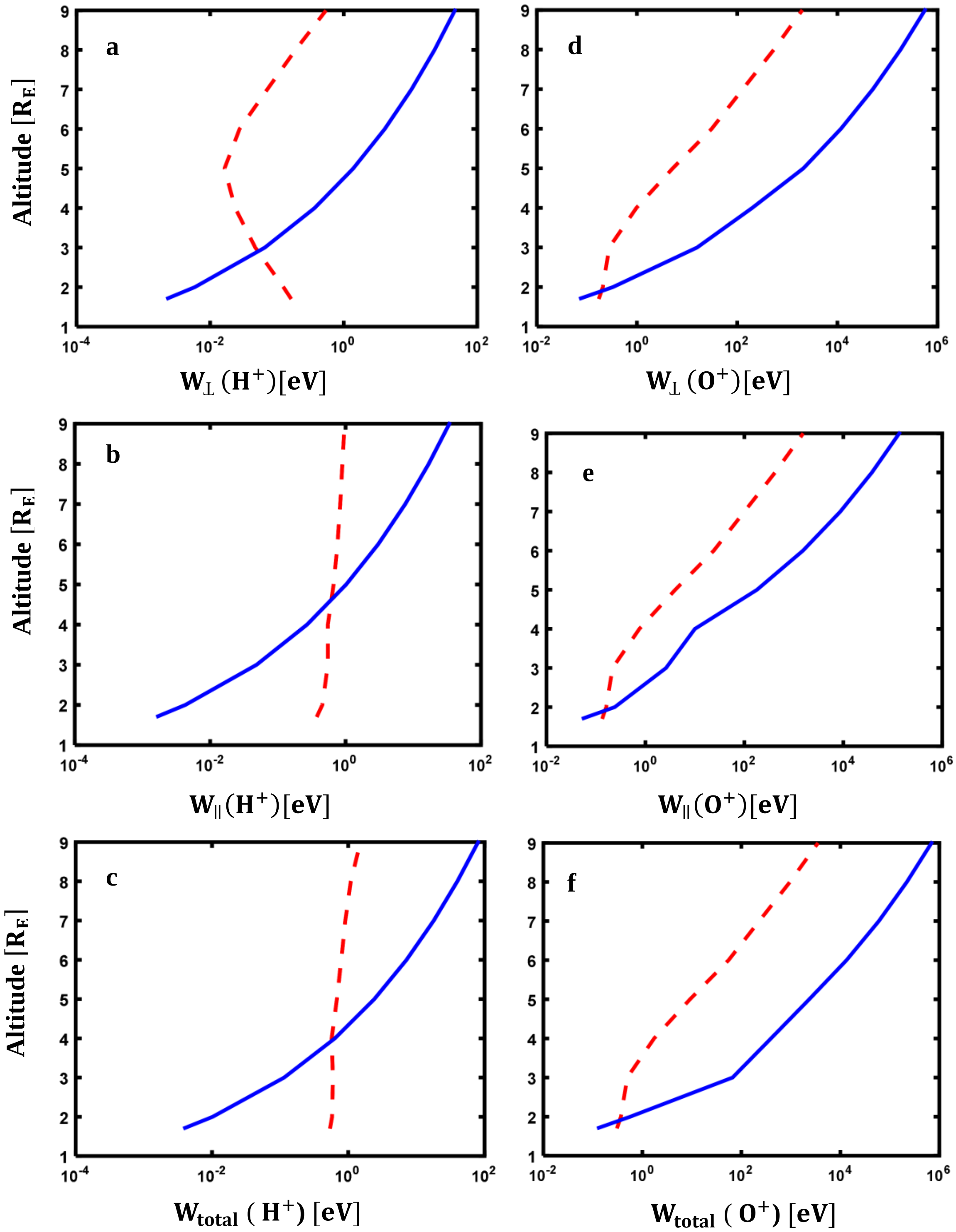

Figure 3.2. Comparison of the estimates of the mean particle theory (blue solid lines) for polar wind conditions with the Monte Carlo calculations (red dashed lines). (right panels, d, e and f) for O^+ ions and (left panels, a, b and c) for H^+ ions and. The mean perpendicular energy $W_\perp$ represented by (panels a and d), mean parallel energy $W_\parallel$

(panels b and e) and total energy (panels c and f) with electromagnetic turbulence wavelengths ($\lambda_{\perp} \to \infty$), and altitude dependent diffusion coefficients.

3.2.c Central Polar Cap and Cusp Regions

To achieve the same goal of calculating the energies, based on the information available to us in both regions (CPC and Cusp) we just calculated the perpendicular energy of O^{+}ions, $W_{\perp}(O^{+})$, this is because the data available for Monte Carlo calculations is the perpendicular temperature only. As for H^{+} ions, we do not have enough data. According to Barghouthi et al. [2016], the perpendicular temperature for O^{+} ions in the CPC and cusp were represented as a function of altitude. There are several curves for perpendicular temperature and each of them is represented according to different diffusion coefficients, part of these curves indicate outcomes according Nilsson diffusion coefficients which we will rely on in our results in this section (i.e., Eq. (18) in the CPC and Eq.(19) in the Cusp) from 1.7 R_E to 15 R_E , and the other curves depends on Barghouthi diffusion coefficient with the velocity dependence introduces. By the estimates of the mean particle theory we use only Eq. (26) to calculate perpendicular energy and compared to Monte Carlo results.

Figure 3.3 represent the mean perpendicular energy of O^{+} ions as a function of altitudes in CPC (left) and Cusp (right) regions , for CPC the $W_{\perp}(O^{+})$ by mean particle theory (blue solid lines) increases smoothly with the ascent to the high altitude from 1.5 R_E to 10 R_E this is due to the increase in the perpendicular diffusion coefficient in that region which depends mainly on the altitude. For Monte Carlo results (red dashed lines) the energy behavior of O^{+} ions also increasing with height altitudes which depend on perpendicular temperature $T_{\perp}(O^{+})$ behavior as shown in Barghouthi et al. [2016] from 1.5 R_E to 15 R_E . We notice in the CPC region that there is a slight difference between the energy curves for both methods at low altitude, and they proceed in a very compatible manner, reaching high altitudes, and then they matches to each other above $9R_E$, it's an excellent agreement. In the cusp region, also the behavior of $W_{\perp}(O^{+})$ increasing directly with altitudes to both methods, there are an excellent agreement between the two approaches as demonstrated by the comparison, at low altitudes below 2.7 R_E the difference between the two methods is very slight, and then the increment begins to match the two behaviors, at 10 R_E a perfect match appeared.

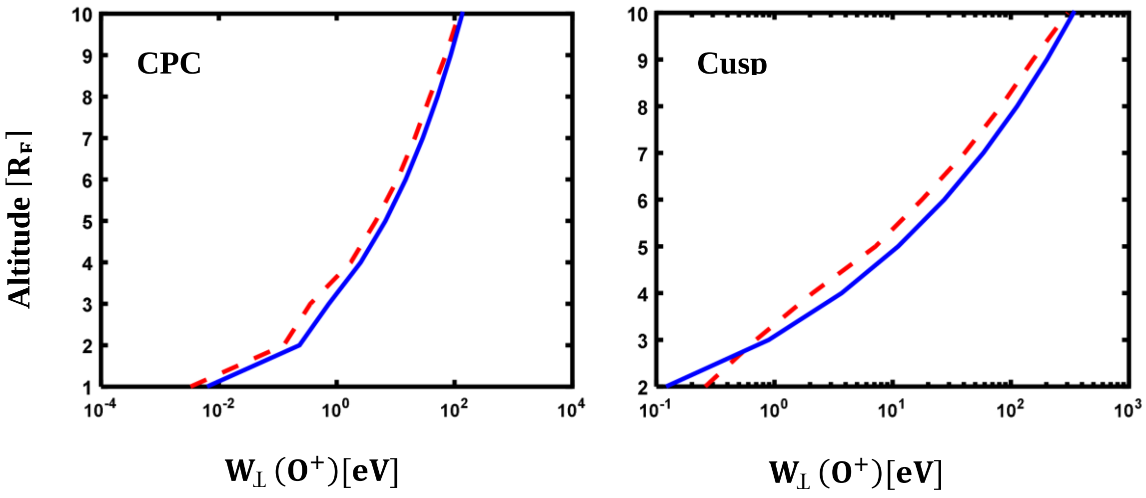

Figure 3.3. Comparison between the Monte Carlo calculations (red dashed lines) and the estimates of the mean particle theory (blue solid lines) for CPC and Cusp regions. Only O^+ ions were considered . mean perpendicular energy $W_\perp$ (left) in CPC region and (right) in cusp region.

3.3 Comparison between Monte Carlo and Mean Particle Theory with altitude and velocity dependent diffusion coefficients $D_\perp(\mathrm{r}, v_\perp)$

As we have seen in the previous section, we made a comparison of the two methods, Monte Carlo method, which is based on simulation results for ($n_i, u_i, T_{i\perp}$ and $T_{i\|}$) for both H^+ and O^+ ions which was applied when the values of characteristic wavelengths for the electromagnetic turbulence approaching to infinity ($\lambda_\perp = \infty$). Thus, the perpendicular diffusion coefficient automatically becomes dependent on altitude only and velocity independent, i.e. $D_\perp(r)$. But in this section we will set specific values for electromagnetic wave lengths ($\lambda_\perp = 1,8,10,20,50\ and\ 100\ km$), that's mean the perpendicular diffusion coefficient turns to be function of perpendicular velocity $v_\perp$ and position (r/R_E) along the geomagnetic field lines. Consequently, the equations of the mean particle theory become $D_\perp(\mathrm{r}, v_\perp)$ dependent instead of $D_\perp(r)$.Thus, it affects the behavior of $W_\perp$, $W_\|$ and W_{total} for

O^+ and H^+ ions outflow . Here we'll see what happens to the energy behavior of O^+ and H^+ in auroral and polar wind regions.

3.3.a Auroral Region with $D_{\perp}(\mathbf{r}, v_{\perp})$

After discussing the new form for the diffusion coefficient and discovered that, in addition to its dependency on altitude, it was also velocity dependent obtained by Barghouthi [2008]. We use this new form of the diffusion coefficient in the estimates of the mean particle theory Eqs. (25), (26) and (27) to see how the behavior of energy ($W_{\perp}$, $W_{||}$ and W_{total}) will be affected when it also depends on velocity for O^+ and H^+ ions. For Monte Carlo calculations Eqs. (7),(8) and (9) also will be used with altitude profiles of H^+ ions moment for various values of $\lambda_{\perp}(\lambda_{\perp} = 1,10, and\ 100\ km)$ [Barghouthi and Atout, 2006] specifically when $\lambda_{\perp} = 10$ km, while for O^+ ions the altitude profiles moment are given by Barghouthi model results for the aurora when $\lambda_{\perp} = 8$ km [Nilsson et al., 2013] with $T_{\perp}(O^+)$ and $T_{||}(O^+)$ are given in electron volte . Figure 3.4 describe energy behavior by using the two techniques, as shown in Figure (3.4a) we found widespread agreement for the mean perpendicular energy for H^+ ions $W_{\perp}(H^+)$ at high altitudes above $5\,R_E$ by two methods, this is due to use of the diffusion coefficient which depends on altitude and velocity where the energy values by using the mean particle theory (blue solid lines) began to approach and largely agree with the Monte Carlo values (red dashed lines) at altitudes higher than $5\,R_E$, meaning that the diffusion coefficient has decreased by ($k_{\perp}v_{\perp}/\Omega)^{-3}$ thus it greatly influences perpendicular energy behavior. The same for O^+ ions where the behavior of the mean perpendicular energy $W_{\perp}(O^+)$ by two methods (Figure.3.4d) are increasing close to each other and they match at high altitudes. We also notice that the energy values by using the mean particle theory are less than their values by using Monte Carlo calculations above $3\,R_E$ this is due to the same reason which is the entry of the velocity coefficient into the equations which reduces the values and becomes closer to Monte Carlo values. For parallel energy for H^+ and O^+ ions ($W_{||}(H^+)$ and $W_{||}(O^+)$) are represents in (Figure.3.4b,3.4e) where the behavior of $W_{||}(H^+)$ increasing smoothly by Monte Carlo method according to the behavior of ($u(H^+)$ and $T_{||}(H^+)$) at $\lambda_{\perp} = 10$ km by Barghouthi and Atout [2006) and not far from the energy path in the mean particle theory which it is quickly escalating to altitude 3.8 R_E then the increase starts slowly due to the effect of the velocity on the diffusion coefficient. For the O^+ ions the Monte Carlo behavior of $W_{\|}(O^+)$ close to matching the estimates of the mean particle theory path at altitudes less than 2 R_E, then they diverge to return to approach at high altitudes. All of these behaviors also inevitably influence again to see the total energy path which would be the sum of both $W_{\perp}$ and $W_{\|}$ by two methods, as appears in (Figure.3.4c,3.4f) for H^+ ions there is a very good agreement at low and high altitudes at $\lambda_{\perp} = 10$ km and increase identically until altitude 2 R_E then a slight divergence occurs, to come back to approach at high altitudes for O^+ ions at $\lambda_{\perp} = 10$ km, due to a decrease in the diffusion coefficient .

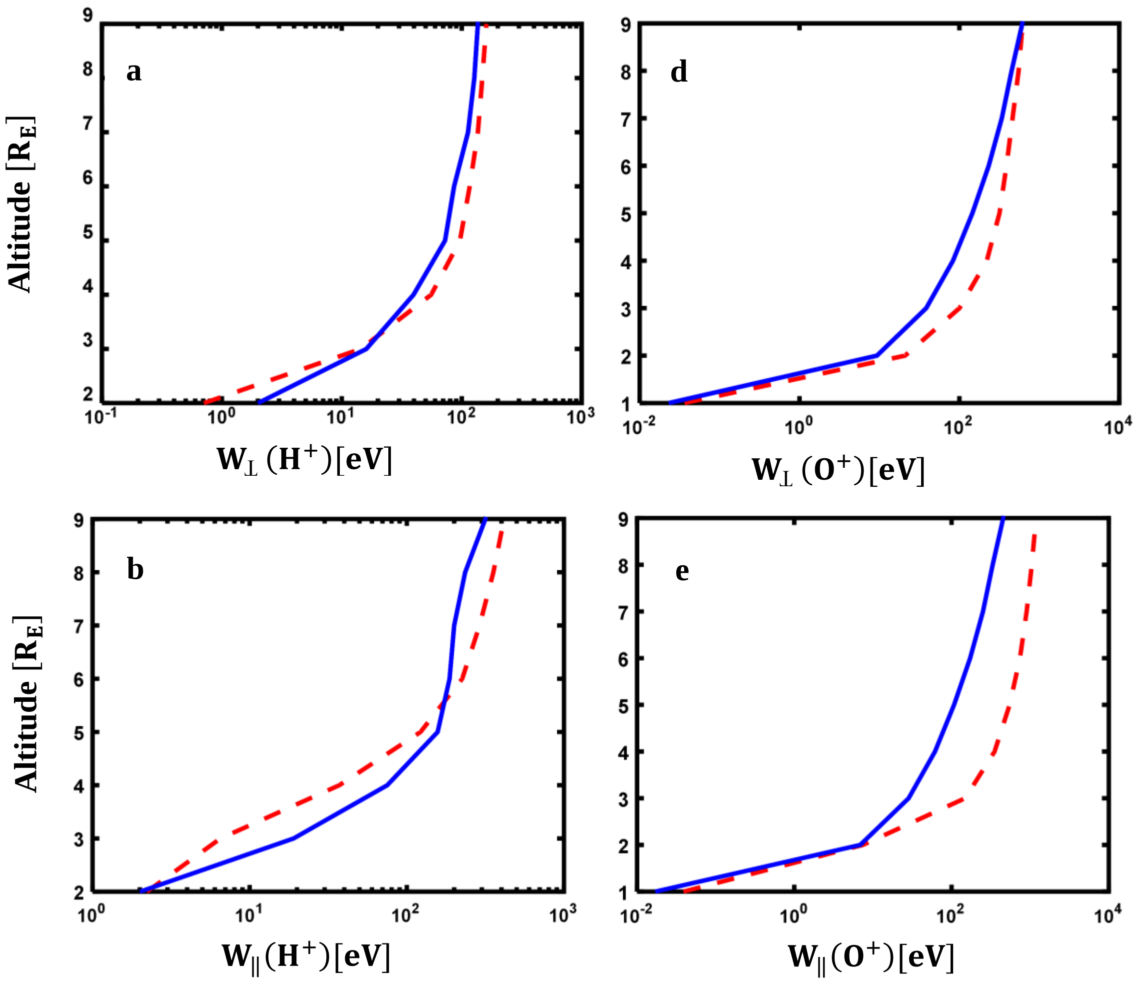

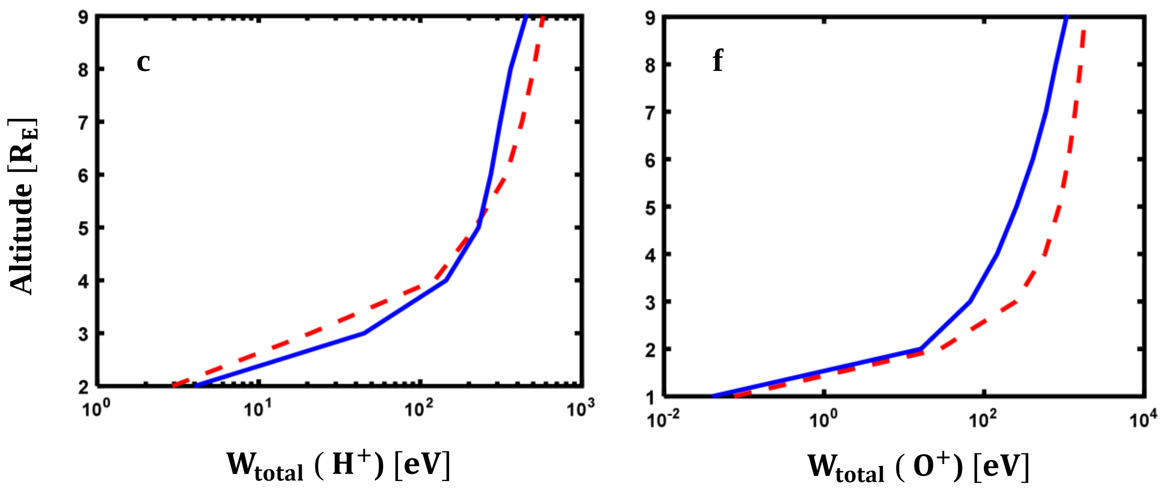

Figure 3.4 . Comparison between the Monte Carlo calculations (red dashed line) and the estimates of the mean particle theory (blue solid lines) in the auroral region when the perpendicular diffusion coefficient $D_\perp$ depends on altitude and velocity with electromagnetic turbulence wavelengths ($\lambda_\perp = 10\ km$) for H^+ ions and ($\lambda_\perp = 8\ km$) , for O^+ ions are given (left panels, a, b and c) and for H^+ ions are given in (right panels, d, e, and f) for O^+ ions. The mean perpendicular energy $W_\perp$ considered here (panels a and d), mean parallel energy $W_{||}$ (panels b and e) and total energy W_{total} (panels c and f).

3.3.b Polar Wind Region with $D_\perp(\mathbf{r}, v_\perp)$

As we previously stated, when the value of perpendicular wavelength of the electromagnetic turbulence changes ($\lambda_\perp = 1{,}8{,}10\ and\ 50\ km$) the perpendicular diffusion coefficient becomes velocity dependent and then the behavior of $D_\perp$ will change as shown in Eq. (20). $D_\perp(\mathrm{r}, v_\perp)$ has greatest value when the perpendicular velocity close to the zero (i.e. $v_\perp \approx 0$)(i.e.($k_\perp v_\perp/\Omega$)< 1) and falls down sharply for high values of $v_\perp$ (i.e. $k_\perp v_\perp/\Omega$)≥ 1) , so the ions (H^+ or O^+) have a tendency to travel away from the region of large diffusion coefficient $D_\perp$ (i.e.($k_\perp v_\perp/\Omega$)< 1) to collect in the region of relatively low diffusion coefficient $D_\perp$ (i.e.($k_\perp v_\perp/\Omega$)≥ 1). Thus, the change in the values of perpendicular wavelength $\lambda_\perp$ appeared clearly in altitude profiles of the different H^+ and O^+ moments in polar wind region in Barghouthi et al.[2011] and Nilsson et al. [2013] and we will benefit from these changes also in the energy behavior of these ions in that region ($W_\perp$, $W_{||}$ and W_{total})

and the subsequent entry of the velocity coefficient into the diffusion coefficient is implicit in the equations of the mean particle theory and how the energy behavior of these ions will become.

Figure 3.5 presents a comparison between Monte Carlo calculations (red dashed lines) and the estimates of the mean particle theory (blue solid lines) at $\lambda_{\perp} = 8$ km for both H^{+} and O^{+} ions in the polar wind region. The behavior of the mean perpendicular energy $W_{\perp}(H^{+})$ for H^{+} ions by Monte Carol method at $\lambda_{\perp} = 8$ km are shown in (Figure. 3.5a) they increase monotonously at altitudes above $5\,R_E$, this due to behavior of perpendicular temperature $T_{\perp}(H^{+})$ where (the WPI has a bigger impact than adiabatic cooling when applied perpendicularly (i.e. WPI is dominant) However, perpendicular temperature $T_{\perp}(H^{+})$ is decreasing with altitude at lower altitudes due to the dominance of the perpendicular adiabatic cooling effect over the WPI) [Barghouthi et al., 2011] therefore this appears clearly in the behavior of $W_{\perp}(H^{+})$ as well. As for the mean particle theory method, there is a continuous increase in energy and at every altitude there is a value for the diffusion coefficient and a value for the velocity and in this case the perpendicular diffusion coefficient $D_{\perp}(r, v_{\perp})$ values are less than its values when the perpendicular wavelength approaching infinity $\lambda_{\perp} \rightarrow \infty$ .Thus, the energy values are generally reduced and become closer to the values by Monte Carlo method at height altitudes. For O^{+} ions the mean perpendicular energy $W_{\perp}(O^{+})$ there are an excellent agreement between two methods, (Figure. 3.5d) shows an almost perfect match at altitudes lower than $2.7\,R_E$ and above $6\,R_E$,. Also the behavior of mean parallel energy of H^{+} ions $W_{||}(H^{+})$ discussed in (Figure. 3.5b) with regard to the Monte Carlo method, we note that there is a slight increase between each altitude and the other, and this depends on the behavior of each (drift velocity $u(H^{+})$ and parallel temperature $T_{||}(H^{+})$ [Barghouthi et al., 2011] where the parallel adiabatic cooling being dominant and the modest influence of WPI increases at high altitudes but decreases at lower altitudes for the case $\lambda_{\perp} = 8$ km [Barakat and Lemaire, 1990], but in mean particle theory there is a rapid increase at altitudes lower than $6\,R_E$ and then it starts decreasing to match the Monte Carlo results at altitude $13\,R_E$, this decrease is due to the decreasing in the values of the perpendicular diffusion coefficient at altitudes above $6\,R_E$ due to its dependence on velocity. The mean parallel energy of O^{+} ions $W_{||}(O^{+})$ (Figure. 3.5e), there is a good agreement between two behavior , they are constantly increasing and it is expected that at great altitudes there will be a match between them this is because the values of energy in the mean particle theory became much lower at $\lambda_{\perp} = 8$ km than their values at $\lambda_{\perp} \to \infty$ but it is constantly increasing to become very close to the Monte Carlo values that we obtained by relying on both drift velocity $u(O^{+})$ and parallel temperature $T_{\parallel}(O^{+})$ behavior which obtained by Barghouthi polar wind model prediction [Nilsson et al., 2013].

As we can see now that all energy calculations have become dependent on changing velocity, this is important and will appear in total energy, where the values for the perpendicular diffusion coefficient still depend on altitude r only without velocity $v_{\perp}$ mostly at lower altitudes that means $(k_{\perp}v_{\perp}/\Omega) < 1$ according to Eq.(20), and then the effect of velocity appears when ($k_{\perp}v_{\perp}/\Omega) \geq 1$ therefore the values become less and decreases by an amount($k_{\perp}v_{\perp}/\Omega)^{-3}$ and this will apply also on the mean particle theory equations Eqs.(25),(26) and (27) at $\lambda_{\perp} = 8$ km. The total energy can be obtained by both methods (Figure. 3.5c) represent the total energy of H^{+} ions W_{total} (H^{+}) as we note the behavior of total energy by mean particle theory increases smoothly with altitudes, it is the result of applying Eq. (27); summation between $W_{\perp}$ and $W_{\parallel}$ but at the same time, it also depends on the velocity because the perpendicular diffusion coefficient depends on the velocity at $\lambda_{\perp} = 8$, as well as the results of the total energy by the of Monte Carlo method which is the result of applying Eq. (9) velocity dependent and increments slightly. As a result of a comparison between the two methods, there is a difference between the two behaviors although at $4\,R_{E}$ there is an intersection between the values, they diverge with the ascent up, but the beauty of that is, the values and behavior of the W_{total} by mean particle theory are much closer to the values of Monte Carlo when it depends on the velocity ($\lambda_{\perp} = 8$) than its values when it does not depend on the velocity ($\lambda_{\perp} \to \infty$) . The behaviors of the total energy of O^{+} ions W_{total} (O^{+}) by two methods represent in last figure (Figure. 3.5f) it is as they are constantly increasing in a compatible and semi-identical manner and it is an excellent result where at higher altitudes, the values converge significantly.

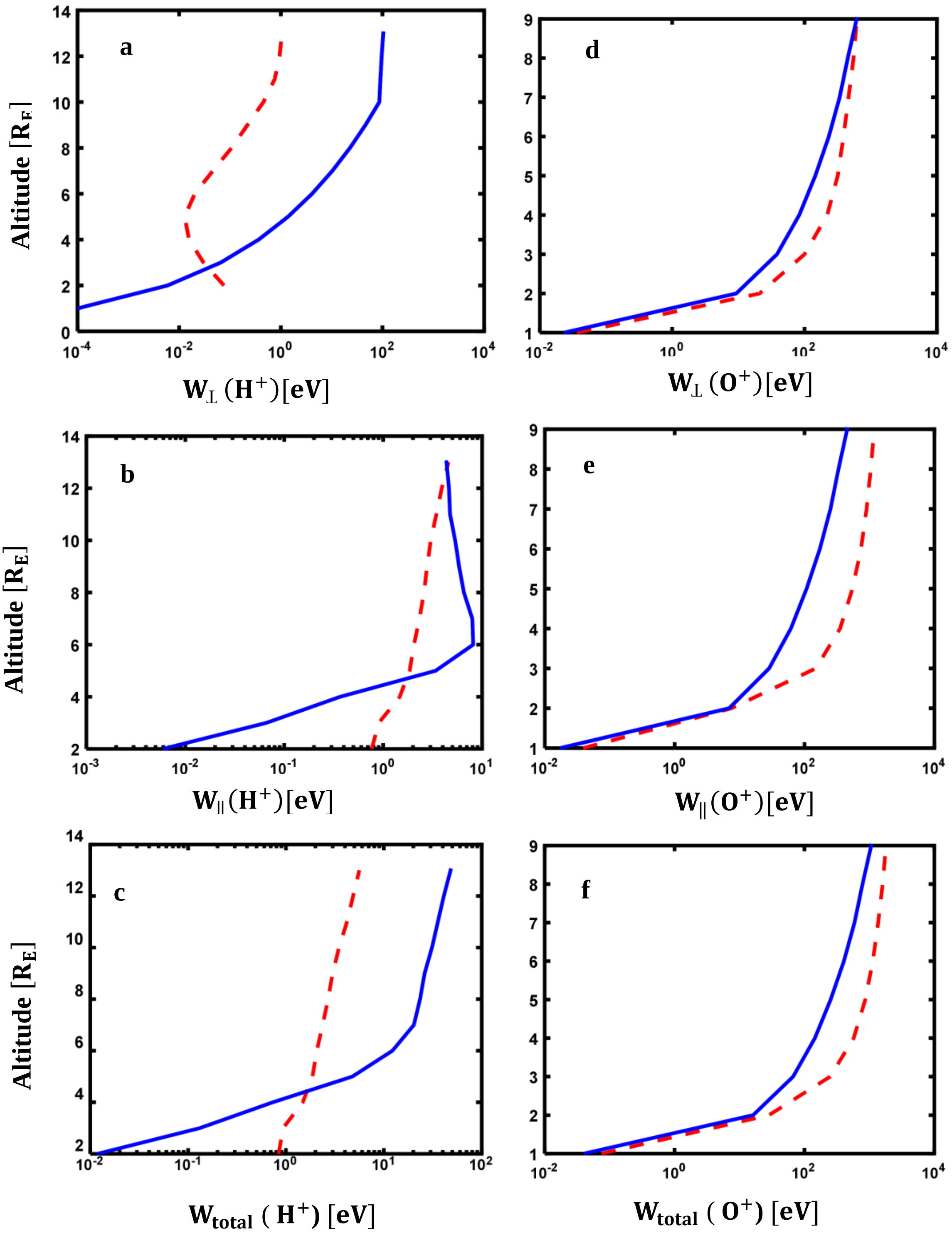

Figure 3.5. Comparison results of Monte Carlo simulations(red dashed lines) with the estimates of the mean particle theory (blue solid lines) by using $D_{\perp}(\mathrm{r}, v_{\perp})$ in calculatins for polar wind region . (left panels, a, b and c) for H^{+} ions and (right panels, d, e and f) for O^{+} ions. The mean perpendicular energy $W_{\perp}$ considered here

(panels a, and d), mean parallel energy $W_{||}$ (panels b, and e) and total energy (panels c and f) with electromagnetic turbulence wavelengths ($\lambda_{\perp} = 8\ km$).

3.4 The behavior of the Mean Particle Theory with various $\lambda_{\perp}$

We previously compared two computational methods by using a set of equations to calculate perpendicular energy $W_{\perp}$, parallel energy $W_{||}$ and total energy W_{total} ; the first of which is the use of Monte Carlo results based on (Altitude profiles of the O^{+} and H^{+} moments for different electromagnetic turbulence wavelengths ($\lambda_{\perp}$) from $\lambda_{\perp} \rightarrow \infty$ to $\lambda_{\perp} = 1$ km and how does a change in $\lambda_{\perp}$ affect on energy, and the second method is the estimates of the mean particle theory which was applied depending on (diffusion coefficient $D_{\perp}$ with altitude and velocity dependence) and this effect was evident in the behavior of energy in the previous sections in both auroral and polar wind regions. By taking advantage of the results of the Monte Carlo simulation in the representation of altitude profiles moments ($n_i, u_i, T_{i\perp}$ and $T_{i||}$) for auroral region given by Barghouthi and Atout [2006] and polar wind region given by Barghouthi et al.[2011], we were able to determine the altitude profiles of energy and how its behavior changes with varying $\lambda_{\perp}$ for both methods.

Figure 3.6 shows the energy behavior in auroral region for H^{+} ions left panel and O^{+} ions right panel starting with perpendicular energy $W_{\perp}$ (Figure 3.6.top) which begins to increase with an upward climb began from $\lambda_{\perp} \rightarrow \infty$ hence the values decrease at specific altitudes which vary with different $\lambda_{\perp}$ values, and all behaviors of $W_{\perp}$ coincide for all values of $\lambda_{\perp}(\lambda_{\perp} = \infty, 100, 10\ and\ 1\ km)$ that is because $k_{\perp}v_{\perp}/\Omega < 1$ for the H^{+} and O^{+} ions at altitudes below 2.5 R_E and 1.5 R_E respectively. In other words, below these altitudes, the impact of finite gyroradius is minimal, the influence of the finite gyroradius becomes more significant as $\lambda_{\perp}$ diminishes. Above these altitudes, the expression ($k_{\perp}v_{\perp}/\Omega)^{-3}$ decreases when $\lambda_{\perp}$ decreases, which in turn causes the diffusion coefficient $D_{\perp}$ to drop , this decrease in the diffusion coefficient leads to a decrease in the perpendicular energy values and this appears clearly in its behavior. The same for parallel energy $W_{||}$ (Figure 3.6.middile) it shows the effect of changing the $\lambda_{\perp}$ values on the behavior of energy at altitudes above $2R_E$ for H^{+}

ions and $1R_E$ for O^+ ions, for example at $\lambda_\perp = 10\ km$ the diffusion coefficient started to depend on the velocity above $4R_E$ for H^+ ions and $2R_E$ for O^+ ions where the energy values are sufficient to be the value $k_\perp v_\perp/\Omega \geq 1$, this encourages the entry of the velocity coefficient into the effect, which in turn affects the diffusion coefficient. The total behavior of $W_\perp$ and $W_\parallel$ represented by total energy W_{total} (Figure 3.6.bottom) as we see, for example, at $\lambda_\perp = 100\ km$ the energy values are very close to the energy values when $\lambda_\perp \to \infty$ for H^+ ions this depends on the Monte Carlo energy values becoming sufficient at high altitudes while for O^+ ions the Monte Carlo values were sufficient at a few altitudes, so the effect of $\lambda_\perp$ appeared at a few altitudes ,we also notice that the behavior in both ways takes approximately the same form (increasing smoothly at low altitudes and starting decreasing with $\lambda_\perp$ decrease so, the Monte Carlo method and the estimates of mean particle theory are excellent comparison methods at low and high altitudes in the auroral region.

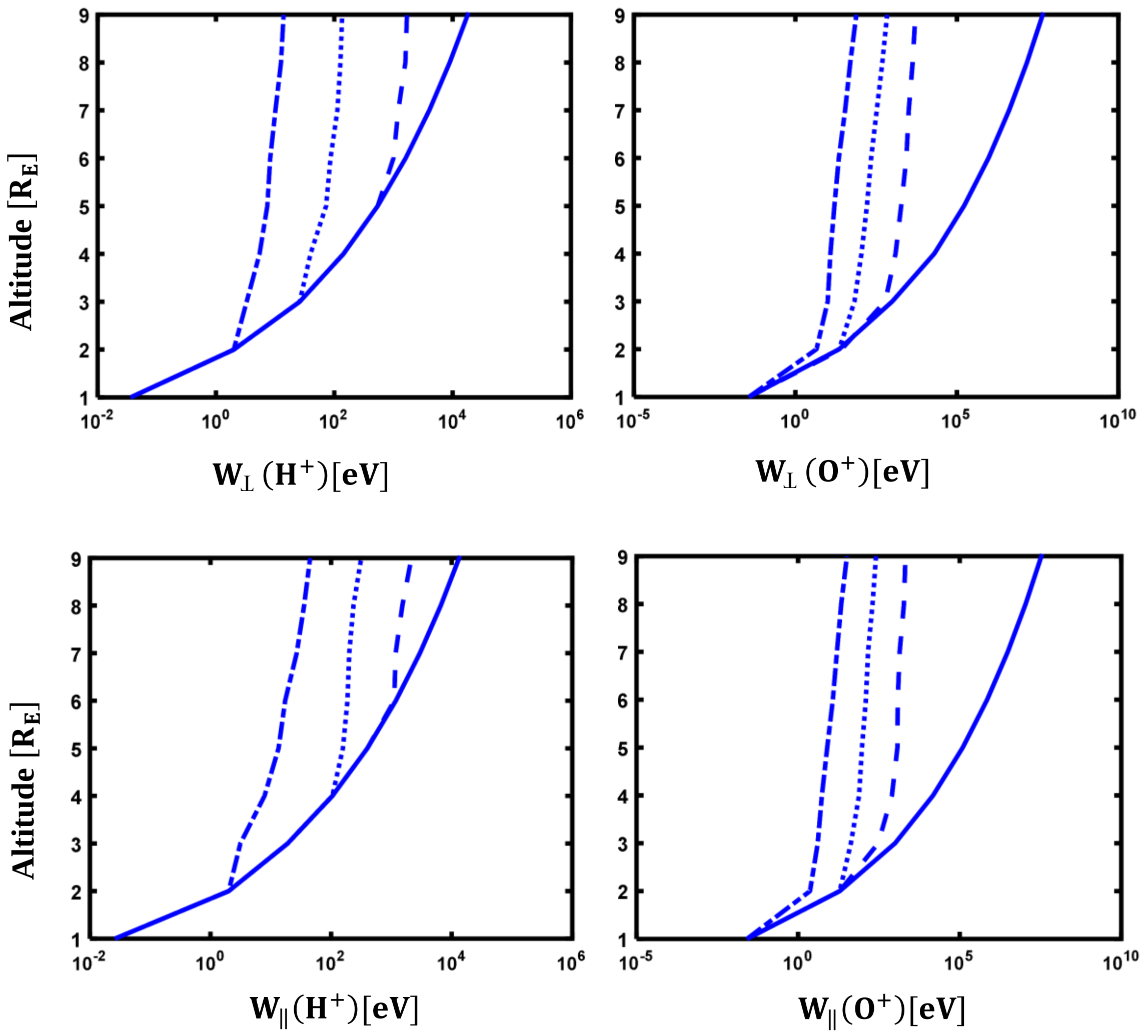

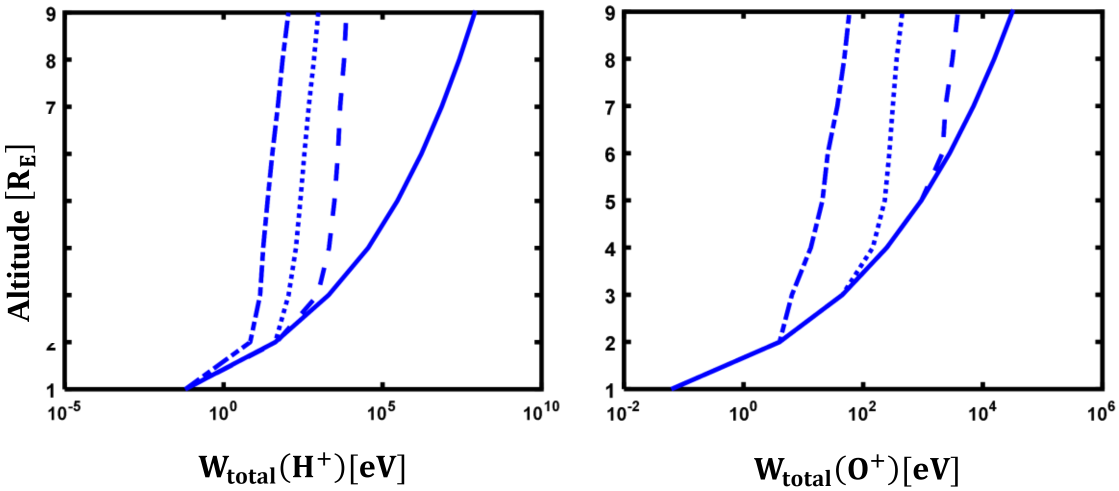

Figure 3. 6. Energy behavior of H^+ ions (left panels) and O^+ ions (right panels) in the auroral region for different electromagnetic turbulence wavelengths ($\lambda_\perp$). The wavelengths considered here are $\lambda_\perp \rightarrow \infty$ (solid line), $\lambda_\perp = 100\ km$ (dashed line), $\lambda_\perp = 10\ km$ (dotted line), $\lambda_\perp = 1\ km$ (dotted dashed line) where the energy represented here are: mean perpendicular energy $W_\perp$ (top panels),mean parallel energy $W_\parallel$ (middle panels) and the total energy W_{total} (bottom panels).

But for polar wind region it turns out more and more which method works best at low altitudes and which one works best at high altitudes where the results appear slightly differently as shown in Figure 3.7 which represents the behavior of $W_\perp$, $W_\parallel$ and W_{total} for H^+ (left panel) ions and O^+ ions(right panel) in the polar wind region by using the estimates of the mean particle theory at different values of $\lambda_\perp(\lambda_\perp = \infty, 50{,}8\ and\ 1\ km)$. For perpendicular energy $W_\perp$ (Figure 3.7.top) at altitudes low than $7R_E$ for H^+ and $3R_E$ O^+ ions respectively, all perpendicular energy behaviors follow the same path with all different $\lambda_\perp$ values and after these altitudes, the tracks begin to separate , this means that the contribution of the velocity fraction in the diffusion coefficient is not negligible and $D_\perp$ becomes velocity dependent, as for the difference that appears here, as we notice at low altitudes for H^+ ions , the energy behavior is shown in detail by the Monte Carlo method, as it begins to decrease and then increases above $5R_E$ based on perpendicular temperature behavior $T_\perp(H^+)$ by Barghouthi et al. [2011] while in the estimates of the mean particle theory method it increases sequentially and there is no effect of the decrease. Therefore, the Monte Carlo method is more valid in use at low altitudes. Also in case of $\lambda_\perp \rightarrow \infty$ and $\lambda_\perp = 50\ km$ have the same behavior by monte Carlo method but in mean particle theory each behavior is appears separately, this makes the mean particle theory more usable at high . For O^+ ions the behavior of this $W_\perp(O^+)$ in order to maintain the first adiabatic invariant μ, a portion of the energy is transferred from the perpendicular direction to the parallel direction during perpendicular adiabatic cooling, which affects how this $W_\perp(O^+)$ behaves by heating O^+ ions in a perpendicular direction. $W_\perp(O^+)$ rises with altitude as a result of WPI's dominance over the perpendicular adiabatic cooling effect. Also, it is evident that when $\lambda_\perp$ decrease $W_\perp(O^+)$ drops as well because $D_\perp$ drops, which in turn causes the heating rate to drop. For parallel energy (Figure 3.7.middel) the effect of velocity in the diffusion coefficient $D_\perp$ starting appear above $3R_E$ for both H^+ and O^+ ions and it decreases with decreasing values of $\lambda_\perp$, also in the case of $\lambda_\perp = 50\ km$ for H^+ ions have the same behavior when $\lambda_\perp \to \infty$ for both ($u(H^+)$ and $T_{||}(H^+)$) [Barghouthi et al.,2011] so the behavior of $W_{||}(H^+)$ by monte Carole method at $\lambda_\perp = 50\ km$ and $\lambda_\perp \to \infty$ it is difficult to differentiate but in the estimates of the mean particle theory it is easy to differentiate between them. The last figure show the total energy (Figure 3.7.bottom) depending on the behavior of both $W_\perp$ and $W_{||}$ for H^+ and O^+ ions which also shows the final conclusion that the Monte Carlo method is more correct and accurate in use at medium and low altitudes. As for high altitudes, the theory method is more accurate and clarifies the behavior.

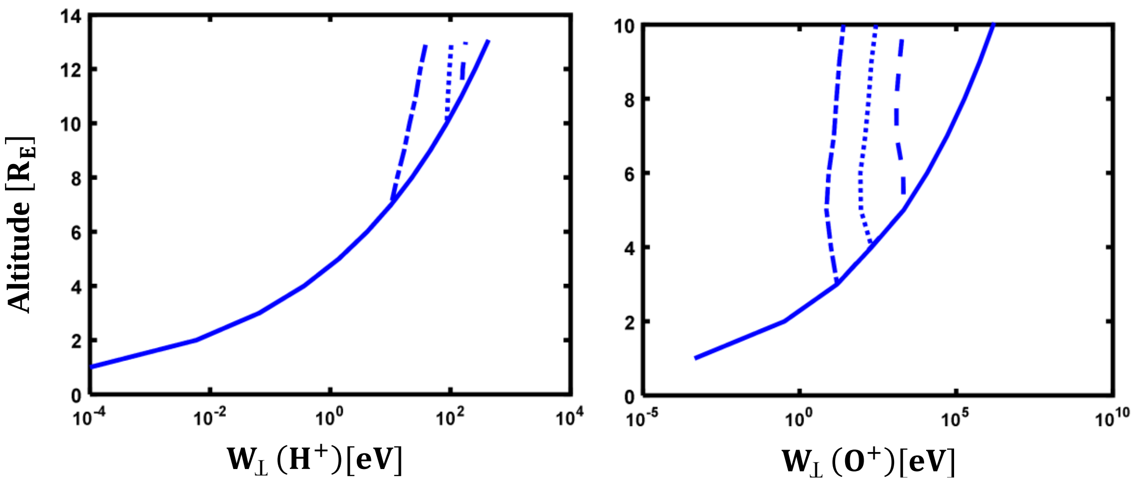

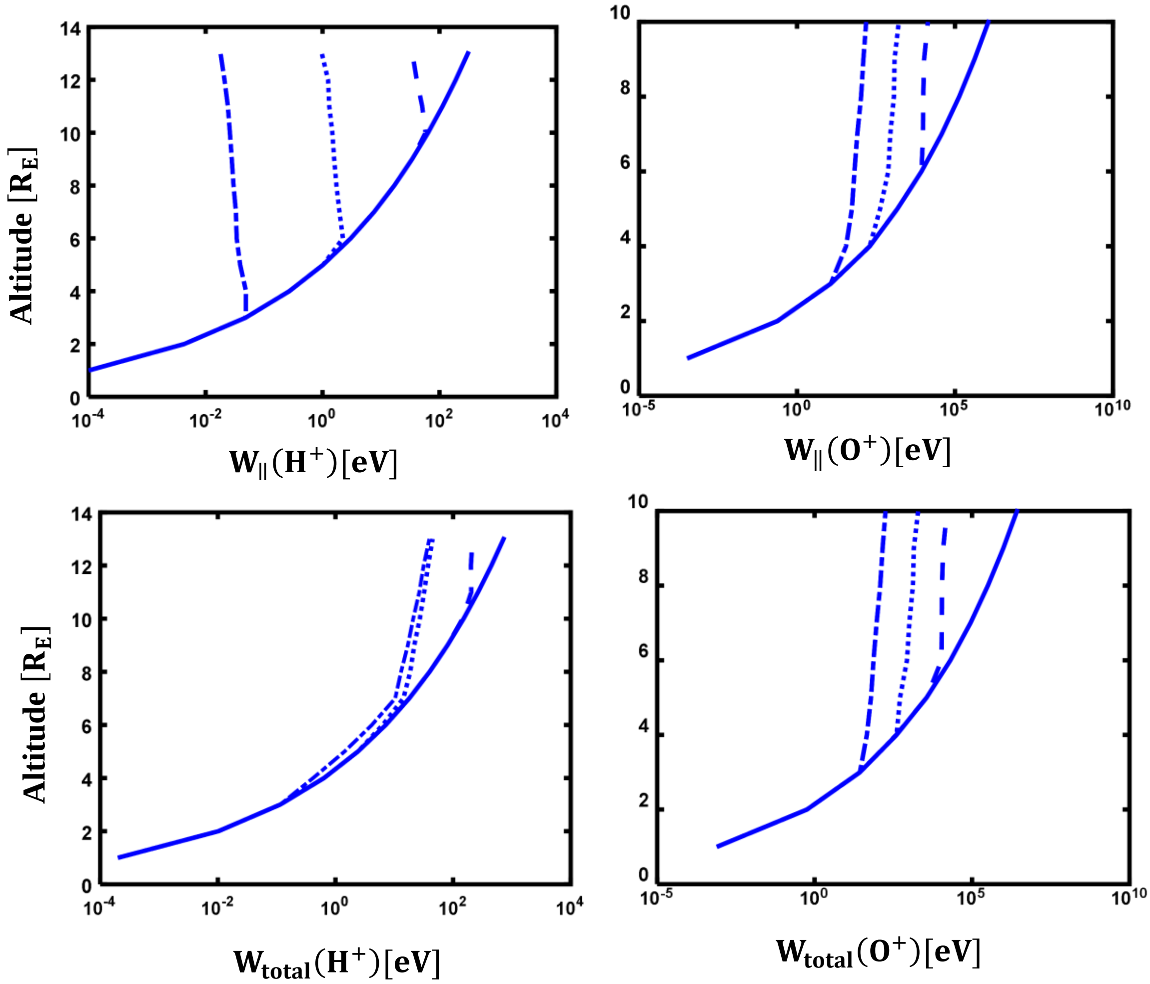

Figure 3.7. Energy behavior of H^+ ions (left panels) and O^+ ions (right panels) in the polar wind region for different electromagnetic turbulence wavelengths ($\lambda_\perp$). The wavelengths considered here are $\lambda_\perp \rightarrow \infty$ (solid line), $\lambda_\perp = 50\ km$ (dashed line), $\lambda_\perp = 8\ km$ (dotted line), $\lambda_\perp = 1\ km$ (dotted dashed line) and the energy considered here are: mean perpendicular energy $W_\perp$ (top panels), mean parallel energy $W_{\|}$ (middle panels) and total energy W_{total} (bottom panels).

3.5 Comparison between Monte Carlo simulations, estimates of The Mean Particle Theory, and available Observations

Barghouthi [2008] compared the simulation output of the Barghouthi model with the corresponding observations for H^+ and O^+ ions outflows in the auroral region, he obtained an excellent agreement, particularly when the typical perpendicular wavelength of the electromagnetic turbulence was 8 km. Also, he observed that there is a broad agreement between the simulation results of the polar wind for this wavelength and the corresponding observations. For these reasons, we chose to have the results of the comparison with the observations also based on the $\lambda_{\perp} = 8\,km$. In this section, we will compare the outcomes of our Monte Carlo simulations, and the estimates of mean particle theory, and available observations obtained from different published articles. For O^{+} ions only and at various altitudes the observations was obtained for parallel velocity, perpendicular temperature and parallel temperature for both polar wind and auroral regions from [Nilsson et al., 2013] and observations for parallel velocity and perpendicular temperature for O^{+} ions in central polar cap and cusp regions from Barghouthi et al. [2016].

In previous sections (Sect. 2 and Sect. 3) we make a comparison between Monte Carlo method and estimates of the mean particle theory by using Eqs. (7,8,9 ,25,26 and 27) based on altitude profiles moments ($n_i, u_i, T_{i\perp}$ and $T_{i\parallel}$) for Monte Carlo method and $D_{\perp}$ for mean particle theory to calculate $W_{\perp}$, $W_{\parallel}$ and W_{total} without any observations, but here according to available information about the observations we can also calculate energy produced of ($n_i, u_i, T_{i\perp}$ and $T_{i\parallel}$) observations ,by using the same Eqs.(7),(8) and (9) at special case $\lambda_{\perp} = 8\,km$ for polar wind and aurora for O^{+} ions and $\lambda_{\perp} \rightarrow \infty$ in central polar cap and cusp regions , and then using this energy generated by these observations as a third method of comparison.

Figure 3.8 presents the results of comparisons in auroral and polar wind regions. The comparison results between Monte Carole method (red dashed lines) and estimates of the mean particle theory (blue solid lines) at $\lambda_{\perp} = 8\,km$ with the observations, in the auroral region (left panels) and polar wind region (right panels), starting with perpendicular energy $W_{\perp}(O^{+})$ for O^{+} ions as we observe at low and high altitudes there is an excellent agreement between Monte Carlo simulations, estimates of mean particle theory and observations, the values of the observations started from $5.7R_E$ where the minimum observed perpendicular energy intersects with the behavior of the perpendicular energy in the two ways which obtained based on the results of the Barghouti model in the auroral region. These results are very good and confirm that the dependence of the diffusion coefficient on the velocity (Barghouthi diffusion coefficients) makes the energy values closer to the observations than its dependence on altitude alone. Also in the polar wind region the behavior of $W_{\perp}(O^{+})$ by two methods are very close to each other and at high altitudes it is appear in the range of observations (between minimum and maximum) values and it is in line with its average , this is an excellent agreement. The same for parallel energy $W_{\parallel}(O^{+})$ (Figure 3.8.middle) for auroral region the minimum curve of observations very close to the results of Monte Carlo calculations and the average curve are closer to the estimates of the mean particle theory , for polar wind two behaviors of $W_{\parallel}(O^{+})$ are closer to the maximum curve of observations it is very good results at $\lambda_{\perp} = 8\ km$.

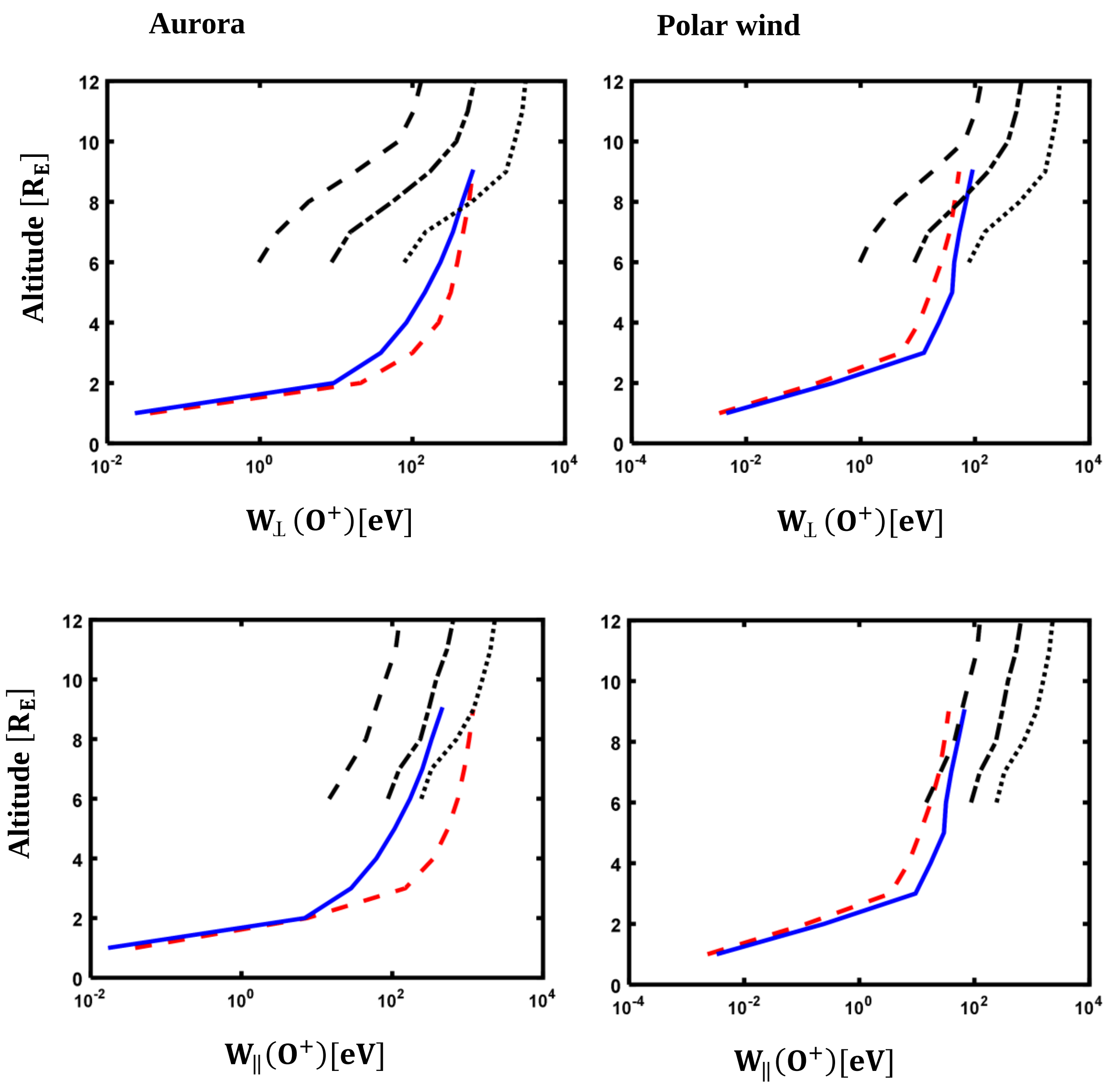

Figure 3.8. Comparison of the estimates of the mean particle theory (blue solid lines) for auroral conditions (left panels) and polar wind conditions (right panels) with the Monte Carlo calculations (red dashed line), in addition to observations, minimum (dott lines) ,avarege (dotted dashed lines) and maximam (black dashed lines) for O^{+}

ions . The mean perpendicular energy $W_{\perp}$ considered here (top) and mean parallel energy $W_{||}$ (bottom) with electromagnetic turbulence wavelengths ($\lambda_{\perp} = 8km$).

In the central polar cap and cusp regions we did the same steps but when $\lambda_{\perp} \rightarrow \infty$ this means the diffusion coefficient $D_{\perp}$ depend only on altitude (Nilsson diffusion coefficients), we also obtained very impressive results, in which it appeared that the behavior of the energy in both methods is in agreement with the observations and the information we have only helped us to find the perpendicular energy in both regions for O^{+} ions and we represented it in the following Figure (3.9).

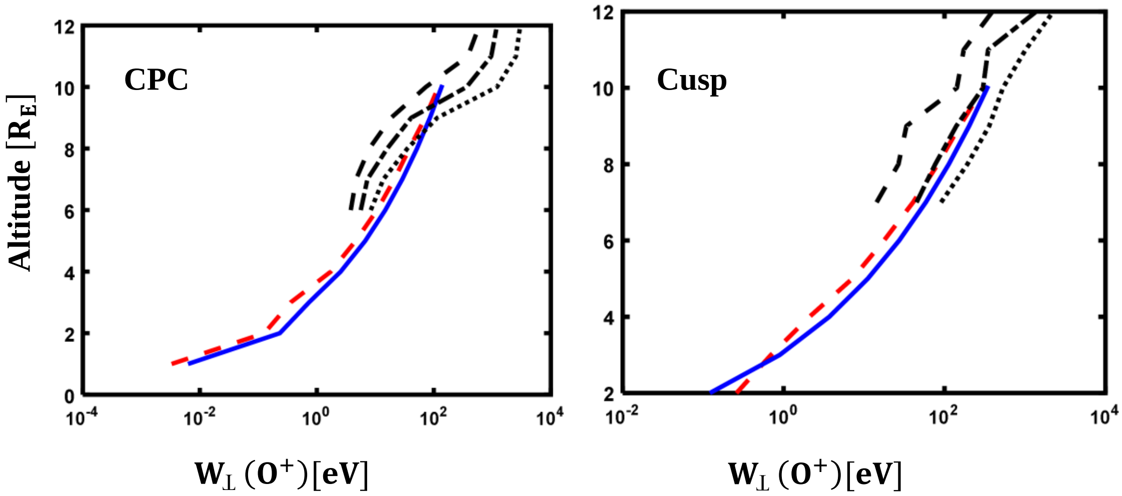

Figure 3. 9 . Comparison of the estimates of the mean particle theory (blue solid lines) for central polar cap conditions (left panel) and cusp conditions (right panel) with the Monte Carlo calculations (red dashed line), in addition to the observations, minimum (dott lines), avarege(dotted dashed lines), and maximam (black dashed lines) for O^{+} ions, mean perpendicular energy $W_{\perp}$ is considered with electromagnetic turbulence wavelengths ($\lambda_{\perp} \rightarrow \infty$).

CHAPTER FOUR

CONCLUSIONS AND FUTURE WORK

We have compared the energy components (mean perpendicular energy $W_\perp$, mean parallel energy $W_{||}$ and total mean energy W_{total} for H^+ and O^+ ions by Monte Carlo calculations as a first method, and the estimates of the mean particle theory as a second method. Also, we investigated how their behavior changes with higher altitudes by adjusting many factors such as the diffusion coefficient $D_\perp$ and its dependence on velocity, in addition to changing the values of characteristic wavelengths for the electromagnetic turbulence $\lambda_\perp$. These comparisons have been applied in various regions based on the information available in each region) altitude profile moments for H^+ and O^+ ions) in auroral region, polar wind region, Central polar cap region and Cusp region. Along with this comparison, it was motivated by observations as a third method of comparison. The main conclusions are as follows:

- In the auroral region and for $\lambda_\perp \to \infty$,there was an excellent agreement between MC simulations and MPT estimates for O^+ ions at all altitudes, and for H^+ ions at altitudes above $2.5R_E$,
- For polar wind region at $\lambda_\perp \to \infty$, there were no agreement between MC simulations and MPT estimates, this means that MPT is not suitable to be used in this region, and MC simulation are more appropriate to be used as shown in Barghouthi et al. [2011] when they compared their results with observations.
- In the last two regions, CPC and Cusp only mean perpendicular energy for O^+ ions behavior was monitored based on the available data, there is a great agreement between the two methods to match the two behaviors at high altitudes.
- When the diffusion coefficient did not depend on the velocity , only on the altitude , its values were large, and therefore the values of the energy generated by applying the Eqs(25),(26) and (27) were also high. But when the diffusion coefficient becomes velocity dependent according to Eq.(6) (i.e. $k_\perp v_\perp/\Omega) \geq 1$), the $D_\perp$ decreasing by amount ($k_\perp v_\perp/\Omega)^{-3}$ which in turn leads to a decrease in energy values in mean particle theory and their estimates become closer to the Monte Carlo behavior .

- For energy behaviors of $W_{\perp}$, $W_{\parallel}$ and W_{total} in both aurora and polar wind regions by mean particle theory with changing $\lambda_{\perp}$, it appears that the general shape is very consistent with the Monte Carlo method as it is at certain altitudes, for example; for the H^{+} and O^{+} ions at altitudes above $2.5\ R_E$ and $1.5\ R_E$ respectively in the auroral region , The effect of velocity appears and each behavior begins to decrease with a decrease in $\lambda_{\perp}$ values.
- Finally, we come to present our available observations as a third method of comparison in the form of minimum , average and maximum values , as it turned out that all results of Monte Carlo and the mean particle theory appeared within the range of these observations, and both methods are close to it, this confirms that the dependence of the diffusion coefficient on altitude and velocity gives appropriate results that are closer to reality and observations and shows the extent of the accuracy of the diffusion coefficients given by Barghouthi [2008] .

For future work, we need to search for more observations in different earth magnetosphere regions in order to have more comparisons and to confirm which diffusion coefficient is more appropriate and which method gives more accurate results when compared to corresponding observations.

REFERENCES

Axford, W.I.: The polar wind and the terrestrial helium budget, J. Geophys. Res., 73, 6855-6859,1968.

Barakat, A. R. and Barghouthi, I. A.: The effects of wave-particle interactions on the polar wind O^+, Geophys. Res. Lett., 21, 2279–2282, 1994a.

Barakat, A. R. and Barghouthi, I. A.: The effect of wave–particle interactions on the polar wind: Preliminary results, Planet. Space Sci., 42, 987–992, doi:10.1016/0032-0633(94)90058-2, 1994b.

Barakat, A. and Lemaire, J.: Monte Carlo study of the escape of a minor species, Phys. Rev. A, 42, 3291–3302, doi:10.1103/PhysRevA.42.3291, 1990.

Barakat, A. R. and Schunk, R. W.: Comparison of Maxwellian and bi Maxwellian expansions with Monte Carlo simulations for anisotropic plasmas, J. Phys. D, 15, 2189-2203, 1982.

Barakat, A. R. and Schunk, R. W.: O^+ ions in the polar wind, J. Geophys. Res., 88, 7887, doi:10.1029/JA088iA10p07887, 1983.

Barakat, A. R. and Schunk, R. W.: Effect of hot electrons on the polar wind, J. Geophys. Res., 89, 977, doi:10.1029/JA089iA11p09771,1984.

Barakat, A. R., Schunk,R. W. and -Maurice,J. P. St.: Monte Carlo calculations of the O^+ velocity distribution in the auroral ionsphere, J. Geophys. Res., 88, 3237–3241, doi:10.1029/JA088iA04p03237,1983.

Barakat, A.R., Schunk, R.W., Moore, T.E., and Waite, J.H.: Ion escape fluxes from the terrestrial high-latitude ionosphere, J. Geophys. Res., 92, 12255–12266, doi:10.1029/JA092iA11p12255, 1987.

Barghouthi, I. A.: Effects of wave particle interactions on $H^+$and O^+ outflow at high latitude; A comparative study, J. Geophys. Res., 102, 22062–22075, 1997.

Barghouthi, I. A.: A Monte Carlo study for ion outflows at high altitude and high latitude: Barghouthi model, J. Geophys. Res., 113, A08209, doi:10.1029/2008JA013274, 2008.

Barghouthi, I. A. and Atout, M. A.: Monte Carlo modeling of toroidal ion distributions and ion temperatures at high altitudes equatorward of the cusp: The effect of finite gyroradius, J. Geophys. Res., 111, A03202, doi:10.1029/2005JA011437, 2006.

Barghouthi, I. A., Abudayyeh, H. A., Slapak, R., and Nilsson, H.: O^+ and H^+ above the polar cap: Observations and semikinetic simulations, J. Geophys. Res. (Space Physics), 121(1), 459-474,2016.

Barghouthi, I. A. and Barakat, A. R.: Comparison between the wave-particle interaction in the polar wind and in the auroral region, Phys. Space Plasmas, 13, 445– 450, 1995.

Barghouthi, I. A., Barakat, A. R., and Persoon, A. M.: The Effects of Altitude-Dependent Wave Particle Interactions on the Polar Wind Plasma, Astrophys. Space Sci., 259, 117–140, doi:10.1023/A:1001569207346, 1998.

Barghouthi, I. A., Ghithan, S. H., and Nilsson, H.: A comparison study between observations and simulation results of Barghouthi model for O^+ and H^+ outflows in the polar wind, Ann. Geophys., 29(11), 2061–2079, doi:10.5194/angeo-29-2061-2011,2011.

Barghouthi, I. A., Nilsson, H., and Ghithan,S.: Comparison between the simulation results of Barghouthi model for ion outflows in the polar wind and auroral regions, J. Assoc. Arab Univ. Basic Appl. Sci., 12(1), 1–10, doi:10.1016/j.jaubas.2012.08.001, 2012.

Barghouthi, I. A., Qatanani, N. A., and Allan, F. M.: Monte Carlo simulation of Boltzmann equation in space plasma at high latitudes, Monte Carlo Methods Appl., 9(3), 201–217, doi:10.1515/156939603322728978, 2003.

Bhardwaj, A., and Gladstone, G. R.:Auroral emissions of the giant planets, Rev. Geophys., *38*(3), 295-353, 2000.

Biddle, A. P., Moore, T. E., and Chappell, C. R.: Evidence for ion heat flux in the light ion polar wind, J. Geophys. Res., 90, 8552, doi:10.1029/JA090iA09p08552, 1985.

Bouhram, M., Dubouloz, N., Malingre, M., Jasperse, J. R., Pottelette, R., Senior, C., Delcourt, D., Carlson, C. W., Roth, I., Berthomier, M., and Sauvaud, J.-A.: Ion outflow and associated perpendicular heating in the cusp observed by Interball Auroral Probe and Fast Auroral Snapshot, J. Geophys. Res., 107(A2), 1023, doi:10.1029/2001JA000091, 2002.

Bouhram, M., Klecker, B., Miyake, W., Rème, H., Sauvaud, J.- A., Malingre, M., Kistler, L., and Blagˇau, A.: On the altitude dependence of transversely heated O^+ distributions in the cusp/cleft, Ann. Geophys., 22, 1787–1798, doi:10.5194/angeo22-1787-2004, 2004.

Bouhram, M., Malingre, M., Jasperse, J. R., and Dubouloz, N.: Modeling transverse heating and outflow of ionospheric ions from the dayside cusp/cleft. 1 A parametric study, Ann. Geophys., 21, 1753–1771, doi:10.5194/angeo-21-1753-2003, 2003a.

Bouhram, M., Malingre, M., Jasperse, J. R., Dubouloz, N., and Sauvaud, J.-A.: Modeling transverse heating and outflow of ionospheric ions from the dayside cusp/cleft. 2 Applications, Ann. Geophys., 21, 1773–1791, doi:10.5194/angeo-21-1773- 2003, 2003b.

Chang, T. and Coppi, B.: Lower hybrid acceleration and ion evolution in the suprauroral region, Geophys. Res. Lett., 8, 1253– 1256, 1981.

Chang, T., Crew, G. B., Hershkowitz, N., Jasperse, J. R., Retterer, J. M., and Winningham, J. D.: Transverse acceleration of oxygen ions by electromagnetic ion cyclotron resonance with broadband left-hand polarized waves, Geophys. Res. Lett., 13(7), 636–639, doi:10.1029/GL013i007p00636,1986.

Collin, H. L., Peterson, W. K., and Shelley, E.G.: Solar cycle variation of some mass dependent characteristics of upfiowing ion beams of terrestrial origin, J. Geophys. Res., 92, 4757-4762, 1987.

Crew, G. B., Chang, T., Retterer, J. M., Peterson,W. K., Gurnett, D. A., and Huff, R. L.: Ion cyclotron resonance heated conics: Theory and observations, J. Geophys. Res., 95, 3959 – 3985, doi:10.1029/ JA095iA04p03959,1990.

Dungey, J. W.: Interplanetary Magnetic Field and the Auroral Zones, Phys. Rev. Lett., 6, 47–48, 1961.

Dungey, J. W., The structure of the exosphere, or adventures in velocity space, in Geophysics: The Earth's Environment, edited by C. DeWitt, J. Hieblot, and A. Lebeau, pp. 503- 550, Gordon and Breach, New York, 1963.

Frey, H. U.: Localized aurora beyond the auroral oval. Rev. Geophys., 45(1), RG1003, doi: 10.1029/2005RG000174,2007.

Ganguli, S. B. and Palmadesso, P. J.: Plasma transport in the auroral return current region, J. Geophys. Res., 92, 8673, 1987.

Ganguli, S. G., Palmadesso, P. J., and Mitchell, H. G.: Effects of electron heating on the current driven electrostatic ion cyclotron instability and plasma transport processes along auroral field lines, Geophys. Res. Lett., 15, 1291, 1988.

Gurnett, D. A., Huff, R. L., Menietti, J. D., Burch, J. L., Winningham, J. D., and Shawhan, S. D.: Correlated low-frequency electric and magnetic noise along the auroral field lines, J. Geophys. Res., 89, 8971–8985, doi:10.1029/JA089iA10p08971, 1984.

Horwitz, J. L., Pollock ,C. J., Moore, T. E., Peterson, W. K., Burch, J. L., Winningham, J. D., Craven, J. D., Frank, L. A., and Persoon ,A.: The polar cap environment of outflowing O^+, J. Geophys. Res., 97, 8361, 1992.

Huddleston, M. M., Pollock,C. J., Wuest, M. P., Pichett, J. S., Moore,T. E., and Peterson, W. K. :Toroidal ion distributions observed at high altitudes equatorward of the cusp, Geophys. Res. Lett., 27(4), 469 – 472, doi:10.1029/1999GL010712,2000.

Lemaire, J. and Scherer, M.: Simple model for an ion-exosphere in an open magnetic field, Phys. Fluids, 14, 1683-1694, 1971.

Lockwood, M., Waite, Jr. J. H., Moore ,T. E., Johnson, J. F. E., and Chappell, C. R.: A new source of suprathermal 04. ions near the dayside polar cap boundary, J. Geophys. Res., 90, 4099, 1985.

Nilsson, H., Barghouthi, I. A., Slapak, R., Eriksson, A. I., and André ,M.: Hot and cold ion outflow: observations and implications for numerical models, J. Geophys. Res., 118(1), 105-117 ,doi: 10.1029/2012JA017975 , 2013 .

Persoon, A.M., Gurnett, D.A., and Shawhan, S.D.: Polar cap electron densities from DE 1 plasma wave observations, J. Geophys. Res., 88, 10123–10136, 1983.

Raitt, W. J. and Schunk , R. W. :Composition and characteristics of the polar wind, Energetic Ion Composition in the Earth's Magnetosphere , 99, 1983.

Retterer, J. M., Chang ,T., Crew, G. B., Jasperse, J. R., and Winningham, J. D.: Monte Carlo modeling of oxygen ion conic acceleration by cyclotron resonance, Phys. Rev. Lett., 59, 148-151, 1987a.

Retterer, J. M., Chang, T., Crew, G. B., Jasperse, J. R., and Winningham, J. D.: Monte Carlo modeling of Oxygen ion conic acceleration by cyclotron resonance with broadband electromagnetic turbulence, Phys. Space Plasmas, 6, 97–111, 1987b.

Retterer, J.M., Chang, T., Jasperse, J.T.: Transversely accelerated ions in the topside ionosphere, J. Geophys. Res., 99, 13,189–13,201, 1994.

Russell, C. T.:The polar cusp, Adv. Space Res., 25(7–8), 1413–1424,doi:10.1016/S0273-1177(99)00653-5, 2000.

Sagdeev, R. Z. and Galeev, A. A.: Nonlinear Plasma Theory (Benjamin, New York), 1969.

Schunk, R. W.: Mathematical structure of transport equations for multispecies flows, Rev. Geophys., 15, 429–445, doi:10.1029/RG015i004p00429, 1977.

Schunk, R.W. and Sojka, J.J.:A three-dimensional time-dependent model of the polar wind, J. Geophys. Res., 94, 8973–8991 ,doi:10.1029/JA094iA07p08973,1989.

Sharp, R. D., Johnson, R. G., Shelley, E. G., and Harris, K. K.: Energetic O^+ ions in the magnetosphere, J. Geophys. Res., 79(13), 1844–1850, doi:10.1029/JA079i013p01844,1974.

Shelley, E. G., Johnson, R. G., and Sharp, R. D.:Satellite observations of energetic heavy ions during a geomagnetic storm, J. Geophys. Res., 77, 6104-6110, 1972.

Shelley, E.G., Peterson, W. K., Ghielmetti ,A. G., and Geiss ,J.: The polar ionosphere as a source of energetic magnetospheric plasma, Geophys. Res. Lett., 9, 941, 1982.

Van Allen, J. A.: Some general aspects of geomagnetically trapped radiation, in Radiation Trapped in Earth's Magnetic Field, Astrophys. Space Sci. Libr., 5, 65–75, 1966.

Waara, M., Nilsson, H., Stenberg, G., Andre, M., Gunell, H., and ´ Reme, H.: Oxygen ion energization observed at high altitudes, ` Ann. Geophys., 28, 907–916, doi:10.5194/angeo-28-907-2010, 2010.

Waara, M., Slapak, R., Nilsson, H., Stenberg, G., André, M., and Barghouthi, I. A.: Statistical evidence for O^+ energization and outflow caused by wave-particle interaction in the high altitude cusp and mantle, Ann. Geophys., 29, 945–954, doi:10.5194/angeo-29-945-2011, 2011.

Winkler, E., -Maurice, J. P. St., and Barakat, A. R.: Results From improved Monte Carlo calculations of auroral ion velocity distributions. J. Geophys. Res., 97, 8399–8423,doi:10.1029/91JA03104,1992.

http://ssdoo.gsfc.nasa.gove.

مقارنة بين محاكاة مونت كارلو , تقديرات نظرية الجسيمات المتوسطة ومشاهدات H^+ و O^+ للتدفقات الخارجة في خطوط العرض العليا.

اعداد الطالبة : مي رجب حلايقة

اسم المشرف : أ.د. عماد البرغوثي

الملخص

في هذا البحث ، نجري مقارنة بين نتائج محاكاة المونت كارلو ، ونظرية الجسيمات المتوسطة ، والمشاهدات المتاحة في مناطق مختلفة من الغلاف المغناطيسي للأرض (aurora, polar wind, central polar cap and cusp) لأيونات H^+ و O^+ التي تتدفق عند خطوط العرض والارتفاعات العالية. نقدم ملفات تعريف الارتفاع لكل من لمتوسط الطاقة العمودية $W_\perp$, متوسط الطاقة المتوازية $W_\parallel$ ومتوسط الطاقة الكلية W_{total}, وتم الحصول على محاكاة مونت كارلو باستخدام نموذج البرغوثي [Barghouthi, 2008] ، كما تم الحصول على تقديرات نظرية الجسيمات المتوسطة باستخدام [Retterer et al., 1987] ، بالإضافة الى المشاهدات التي تم الحصول عليها من العديد من الدراسات المتاحة. ونتيجة للمقارنات في تلك المناطق المختلفة وجدنا أن: 1) محاكاة المونت كارلو ونظرية الجسيمات المتوسطة تعطي نتائج مماثلة في منطقة aurora ولا يوجد أي اتفاق في منطقة polar wind , 2) تعطي المقارنة مع المشاهدات المتوفرة في منطقة polar wind و منطقة aurora اتفاقًا ممتازًا في aurora واتفاقًا جيدًا في polar wind ,3) من المناسب استخدام معاملات الانتشار التي تعتمد على الارتفاع والسرعة $D_\perp(r, v_\perp)$ في مناطق aurora و polar wind والذي كان سببا في الحصول على نتائج معقولة, 4) في مناطق ال central polar cap وcusp ، حصلنا على اتفاق ممتاز لكل من طرق المقارنات السابقة والمشاهدات ، 5) استنادا الى نتائج هذه المقارنات يمكننا أن نتحلى بأن طول موجة الموجة الكهرومغناطيسية الموجودة في تلك المناطق يبلغ 8 km.